International Journal of Microwave and Wireless Technologies

cambridge.org/mrf

A metamaterial absorber based high gain directional dipole antenna

Sarin Valiyaveettil Pushpakaran[1], Jayakrishnan M. Purushothama[2], Manoj Mani[2], Aanandan Chandroth[2], Mohanan Pezholil[2] and Vasudevan Kesavath[2]

[1]Department of Electronics, Government College Chittur, Palakkad, Kerala-678104, India and [2]Centre for Research in Electromagnetics and Antennas, Cochin University of Science and Technology, Cochin-22, Kerala, India

Research Paper

Cite this article: Pushpakaran SV, Purushothama JM, Mani M, Chandroth A, Pezholil M, Kesavath V (2018). A metamaterial absorber based high gain directional dipole antenna. *International Journal of Microwave and Wireless Technologies* 1–7. https://doi.org/10.1017/S1759078718000454

Received: 23 August 2017
Revised: 20 February 2018
Accepted: 21 February 2018

Keywords:
Absorbers; dipole antenna; metamaterials; reactive to propagatingconversion

Author for correspondence:
Sarin Valiyaveettil Pushpakaran, E-mail: sarincrema@gmail.com

Abstract

A novel idea for generating directional electromagnetic beam using a metamaterial absorber for enhancing radiation from a microwave antenna in the S-band is presented herewith. The metamaterial structure constitutes the well-known stacked dogbone doublet working in the absorption mode. The reflection property of the dogbone metamaterial absorber, for the non-propagating reactive near-field, is utilized for achieving highly enhanced and directional radiation characteristics. The metamaterial absorber converts the high-spatial reactive spectrum in the near-field into propagating low-spatial spectrum resulting in enhanced radiation efficiency and gain. The gain of a printed standard half-wave dipole is enhanced to 10 dBi from 2.3 dBi with highly directional radiation characteristics at resonance.

Introduction

Electromagnetic wave propagation through periodic guiding structures has been a constant source of inspiration for research community over the decade [1]. Even though the transmission and reflection spectra could be controlled by periodically loading inductors and capacitors in a transmission line, the invention of metamaterials has given an additional degree of freedom for controlling electromagnetic wave propagation [2]. The unusual dispersive nature of periodic metamaterial elements gives rise to different propagation scenarios like negative refractive index, near-field lensing etc [3]. In left-handed materials, phase and group velocities are anti-parallel to each other and a variety of studies has been focused on the phenomenon in microwave and THz regime [4,5].

The ability to exercise independent control over the phase and magnitude of reflection and transmission coefficients gives an interesting outlook and attraction to metamaterials in contrast to the conventional materials [6,7]. Negative refractive index property could be easily implemented using the stacked metal slab pairs [8,9]. The metal slab pairs exhibit both electric and magnetic resonances. Both these resonances can be controlled and could be merged each other yielding negative refractive index behavior. Another convenient method is to use the stacked dogbone metamaterial in which independent control of resonances could be easily achieved [10]. There is a close correspondence between the transmission characteristics of stacked perforated arrays [11] and stacked dogbone metamaterials [12].

Among the numerous applications of metamaterials, an important feature is electromagnetic absorption using engineered electric and magnetic inclusions. The basic theory behind absorption is to make equal values of electric and magnetic dipole polarizabilities on the composite [13]. In finite difference time domain (FDTD) simulations, perfectly matched layer (PML) boundary is used for electromagnetic wave absorption [14]. It is well known that an electromagnetic source generates both propagating as well as evanescent waves. Propagating plane waves are responsible for far-field radiation and the evanescent wave contains sub-wavelength information about the source and is decayed exponentially within the near-field of the excitation. PML layer absorbs energy contained in the propagating spectrum of the electromagnetic wave whereas evanescent wave undergoes reflection from the boundary [15]. Recently, Tretyakov et. al. introduced the concept of conjugately matched layer (CML) for matching the high-spatial reactive power in addition to the propagating ones [16]. Unlimited power reflection can be achieved by placing random sub-wavelength particles above the CML layer. Therefore, the interaction of evanescent and real propagating waves with matter is of great concern in metamaterial research.

An evanescent wave behaves differently with matter as compared with a real propagating wave [17]. The real part of refractive index adds phase shift for a propagating wave and the imaginary part of refractive index introduces energy dissipation in the form of absorption. For an evanescent wave, the real part of refractive index introduces absorption and the imaginary part is responsible for phase shift. Therefore, the imaginary part of refractive index causes reflection from the material sample under consideration. There is a close resemblance between

CAMBRIDGE UNIVERSITY PRESS

the motion of electrons under the potential function and electromagnetic wave interaction with matter [17].

In this paper, the reflection offered by the artificial dogbone metamaterial absorber is used for achieving greatly enhanced and directional radiation characteristics from a standard printed dipole antenna. The absorber converts the reactive high-spatial spectrum existing in the near-field of the antenna into propagating low-spatial ones, which greatly enhances the radiation performance of the antenna. Simulation studies are performed using CST Microwave Studio and experiments are validated using the Agilent PNAE8362B network analyzer. Radiation performance of the proposed antenna is compared with a conductor backed dipole and the effect of loading height on antenna performance are also studied.

Theory and characterization of the metamaterial

The metamaterial unit cell considered here is the stacked copper plates made in the shape of Dogbone cell etched on a low-cost epoxy substrate with dimensions as shown in Fig. 1. The epoxy substrate is characterized by a dielectric constant 4.4 with thickness 0.8 mm. The final fabricated array contains 10×10 elements with stacking height denoted by d_z. The metamaterial array is fabricated using the standard photo-lithographic etching techniques.

When a time-varying electromagnetic wave with polarization along Y-axis is applied as shown in Fig. 1, resonance can be excited on the metamaterial and the nature of resonance could be controlled by varying the stack thickness. Commercially available electromagnetic simulation tools are equipped with functionalities to perform unit cell simulations to extract reflection and transmission coefficients of the entire array. For that, perfect electric boundary condition is applied on the upper and lower faces of the unit cell, perpendicular to the Y-axis and perfect magnetic boundary is applied on the left- and right-faces of the unit cell, perpendicular to the X-axis. Waveguide ports are assigned on the air extended front and back faces of the unit cellwith electric field orientation along Y-axis. This will allow the propagation oftransverse electromagnetic waves along Z-direction with polarization along Y-axis.

The variation in reflection, transmission, and absorbance of the structure with stacking height d_z is given in Fig. 2. It is evident that increase in stacking thickness enhances the transmission coefficient at resonance for normal incidence. For $d_z = 1$ mm, the low values of reflection and transmission coefficients at resonance (3.1 GHz) indicate that the metamaterial structure is acting as an electromagnetic absorber. This case gives maximum absorption and the absorbance is found to be nearly 80% at resonance.The absorbance (A) of the structure has been calculated from the transmittance (T) and reflectance (R) using the relation, $A(\omega) = 1\text{-}T(\omega)\text{-}R(\omega)$.

The structure shows near unity resonant transmission for $d_z =$ 4 mm onwards and this mode has been used for achieving left-handed transmission behavior for microwave applications [9,10,18]. Left-handed transmission peaks are associated with

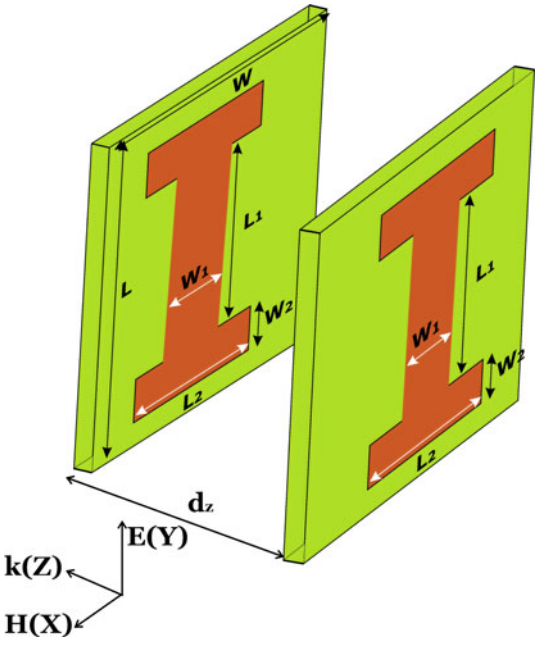

Fig. 1. Unit cell of the dogbone doublet metamaterial slab ($L_1 = 18$ mm, $L_2 = 12$ mm, $W_1 = 4$ mm, $W_2 = 2$ mm, $L = W = 24$ mm).

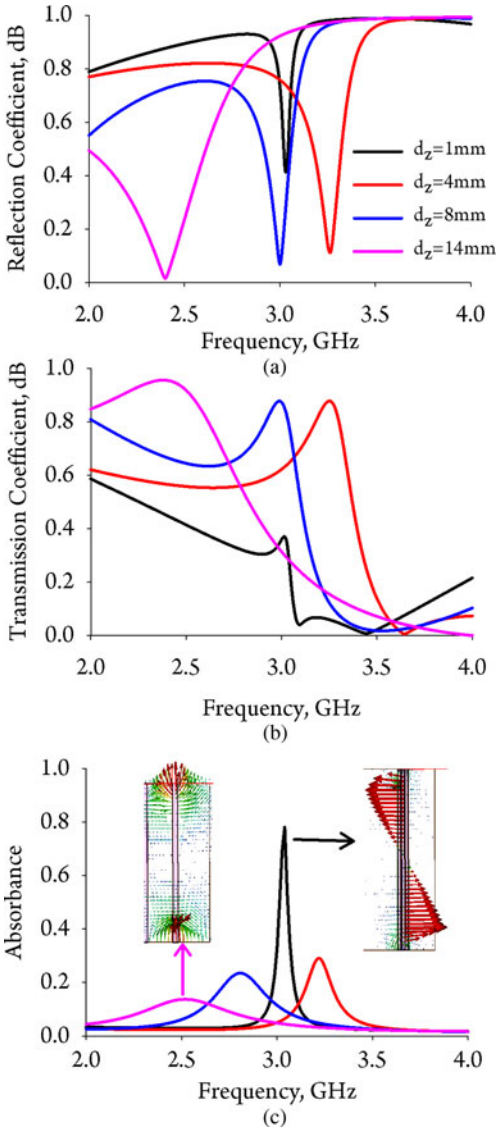

Fig. 2. Effect of stack thickness on (a) reflection, (b) transmission coefficients, and (c) absorbance with electric field distributions in the inset.

minimum absorbance as dictated in Fig. 2(c). The power transmission enhancement of cut- wire pairs finds applications in using this metasurface as a superstrate for enhancing the radiation performance of dipole antennas [18]. The side view of simulated electric field distributions on the unit cell for $d_z = 1$ mm and $d_z = 14$ mm are also shown in the inset of Fig. 2(c). It is noted that for a lower stacking height, E_z component of electric field is dominating over the E_y component. So initial increase in d_z decreases the capacitance between the plates and resonance is shifted towards the higher side. For higher stacking heights, magnetic resonance is excited and the E_y component of electric field is dominating over the E_z component. Hence, for higher stacking heights, increase in d_z lowers the resonant frequency of the metamaterial. This is due to the fact that magnetic resonance is excited due to the anti-parallel currents on the lower and upper metallic plates of the metamaterial unit cell.

The effective material parameters of the medium are extracted using the Ziolkowski method [19] and the retrieved values are depicted in Fig. 3. Since the study is focused on the absorption resonance, the parameters for $d_z = 1$ mm is considered here. It is evident that the structure shows strong permittivity resonance yielding negative values of permittivity after resonance. Since magnetic dipole resonance is absent, the structure could be identified as an artificial dielectric exhibiting negative permittivity after resonance. The positive permittivity peak before resonance can be used for superstrate applications. An increase in stacking thickness further excites magnetic response and shows left-handed transmission peaks. Further studies in this regard have been omitted for brevity. Corresponding to the electric resonance, the imaginary part of permittivity attains a huge value resulting in electromagnetic absorption for propagating waves. It is well known that increasing the value of imaginary part of permittivity enhances absorption for regular propagating waves.

Maximizing absorption is a challenging task while dealing with evanescent waves as the presence of imaginary part in permittivity scatters the evanescent spectrum of an incident wave. Consider an evanescent wave traveling from air to an artificial dielectric characterized by real and imaginary part of permittivity ($\varepsilon_m = \varepsilon'_m\text{-}j\varepsilon''_m$). The Poynting vector on the artificial dielectric medium is given by [17],

$$< S \geq \left[\varepsilon'_m k_x, 0, \varepsilon''_m k'_z\right] \frac{c^2}{8\pi\omega|\varepsilon_m|^2} |T|^2 H_0^2 e^{-2k'_z} e^{-2zk'_z}, \quad (1)$$

where T is the Fresnel transmission coefficient, H_0 is the magnetic field of the incident beam, K_x is the transverse wave number, K_z is the longitudinal wave number and, ω is the angular frequency. For a reactive near-field, transverse oscillations would be dominant and hence, absorption can be maximized when the imaginary part of permittivity becomes zero. Increasing the value of imaginary part of permittivity decreases absorption and enhances reflection. It is also noted that reactive electromagnetic waves incident on a metal at optical frequencies gives anomalous reflection [20], in which the magnitude of reflection coefficient is greater than unity. We are experimentally showing that the anomalous reflection is due to the reactive to propagating wave conversion offered by the artificial dielectric. In this paper, the spectral conversion offered by the dogbone metamaterial absorber is utilized for enhancing the radiation performance of a microwave antenna. As per the theory, when the dogbone metamaterial absorber is placed in the vicinity of the dipole antenna, it will naturally absorb the propagating spectrum and reflects the high-spatial frequency spectrum impinging on the surface. The reflection is associated with the corresponding propagating wave conversion resulting in enhanced radiation performance.

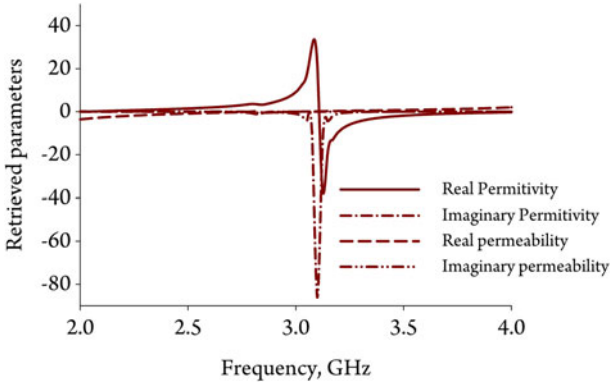

Fig. 3. Retrieved material parameters for $dz = 1$ mm.

Practical realization

For practical realization of the above concept, we have used a planar half-wave dipole antenna printed on an epoxy substrate with dimensions $L_d X W_d$. The antenna is fed using a microstrip to slot line transition in order to avoid back currents on the feed cable of the network analyzer.

The geometrical parameters of the antennas are given in Fig. 4. The configuration of free-standing printed dipole is shown in Fig. 4(a). A Sub Miniature version-A connector is used for feeding the microstrip part of the balun structure. The dipole antenna is loaded at a height of $h_1 = 14$ mm$(0.15\lambda_0)$ above the dogbone metamaterial absorber layer as shown in the side view as Fig. 4 (b). For practical realization, the antenna element is supported using a perspex holder. The metamaterial absorber array occupies an overall area of $206(2.14\lambda_0)X160(1.66\lambda_0)$ mm^2.

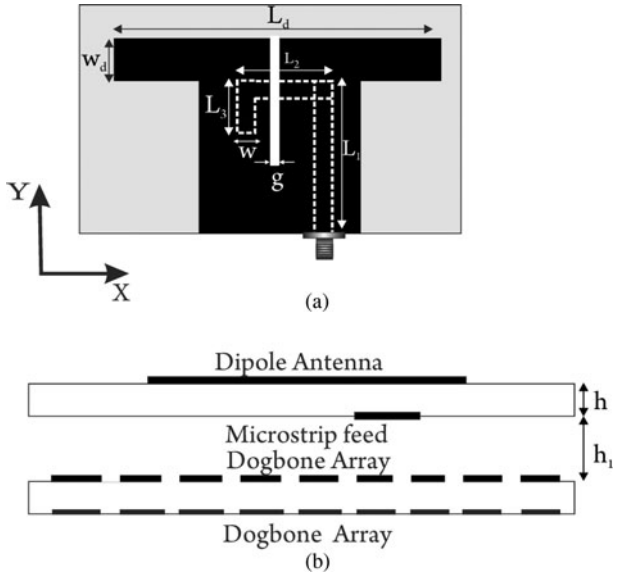

Fig. 4. Geometry of the artificial dielectric backed dipole antenna (a) Dimensions of the dipole used and (b) side view of the final antenna ($L_d = 36.5$ mm, $W_d = 5$ mm, $L_1 = 18$ mm, $L_2 = 10$ mm, $L_3 = 8$ mm, $w = 3$ mm, $h_1 = 14$ mm, $h = 0.8$ mm, and $g = 0.5$ mm).

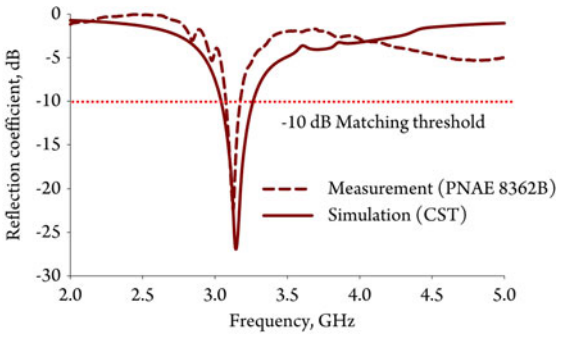

Fig. 5. Magnitude of reflection coefficient of the antenna ($h_1 = 14$ mm).

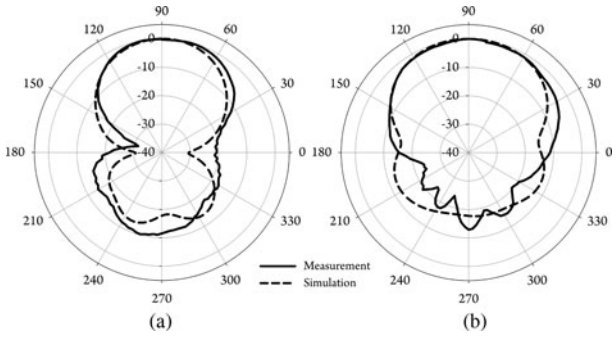

Fig. 6. Measured and simulated radiation patterns of the antenna (a) *E*-plane pattern and (b) *H*-plane pattern.

The simulated and measured reflection characteristics of the proposed absorber backed dipole antenna are shown in Fig. 5. The simulation and measurement are in good agreement with each other. The resonant frequency of the antenna is found to be 3.12 GHz with a reflection coefficient of −23 dB at resonance. The 2:1 voltage standing wave ratio (VSWR) bandwidth of the proposed design is 3.52% around resonance whereas the free-standing dipole shows an improved bandwidth of 16% at resonance. The red dotted line indicates the commonly used −10 dB impedance matching threshold level.

Far-field measurements are recorded in an anechoic chamber using an ultra wide band horn antenna. The distance between the metamaterial loaded antenna and the horn antenna is fixed as 4 m. Maximum power received from the antenna under test is noted in the boresight direction and a THRU calibration is made for normalization of the radiated power. The antenna is rotated using a computer controlled turn table assembly and the received power is recorded for the two principal planes. The measured and simulated normalized radiation patterns of the antenna in the two principal planes are shown in Fig. 6. The small discrepancies are accounted due to the measurement tolerance. The measurements confirm the directional radiation characteristics of the metamaterial loaded design. The 3 dB beam width is found to be 72° for the *E*-plane and 93° for the *H*-plane. Cross-polar isolation is found to be −25 dB for the *H*-plane pattern and −18 dB for the *E*-plane pattern. The design exhibits a front to back ratio of −12 dB at resonance. The gain of the antennas is measured using the standard gain comparison method. In the measurement, the loaded dipole shows more than three-fold increase in gain from 2.3 dBi to 10 dBi, in comparison with the unloaded free-standing case. Wheeler-Cap method has been used for the measurement of

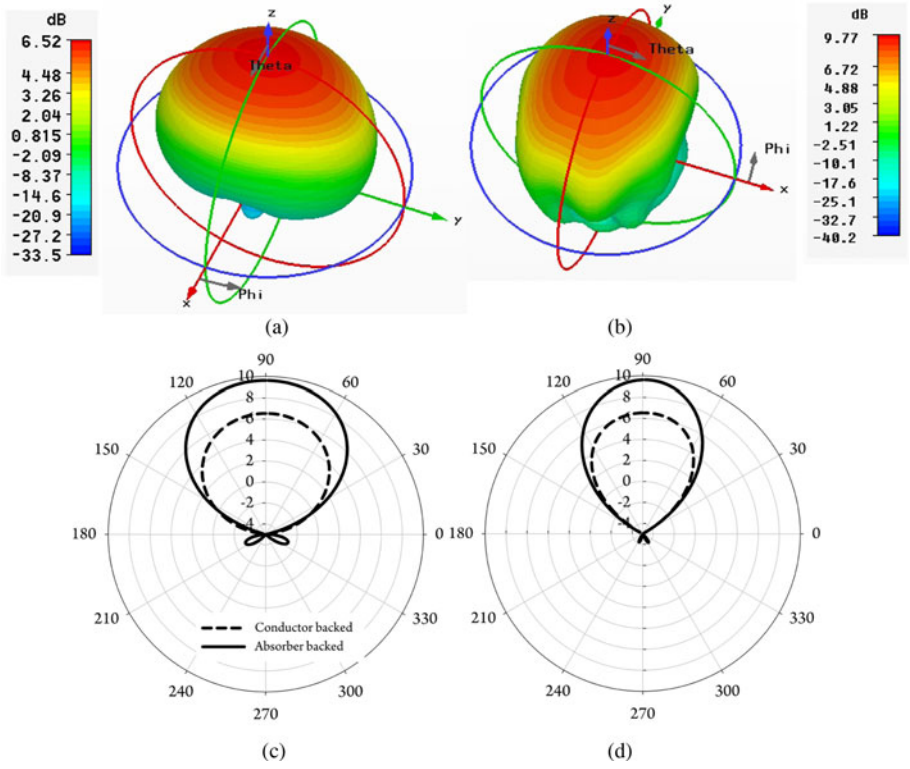

Fig. 7. Comparison of gain patterns of a conductor backed dipole and the absorber backed dipole (a) 3D gain pattern of conductor backed dipole antenna, (b) 3D gain pattern of metamaterial backed dipole, (c) comparison of *H*-plane patterns and (d) comparison of *E*-plane patterns.

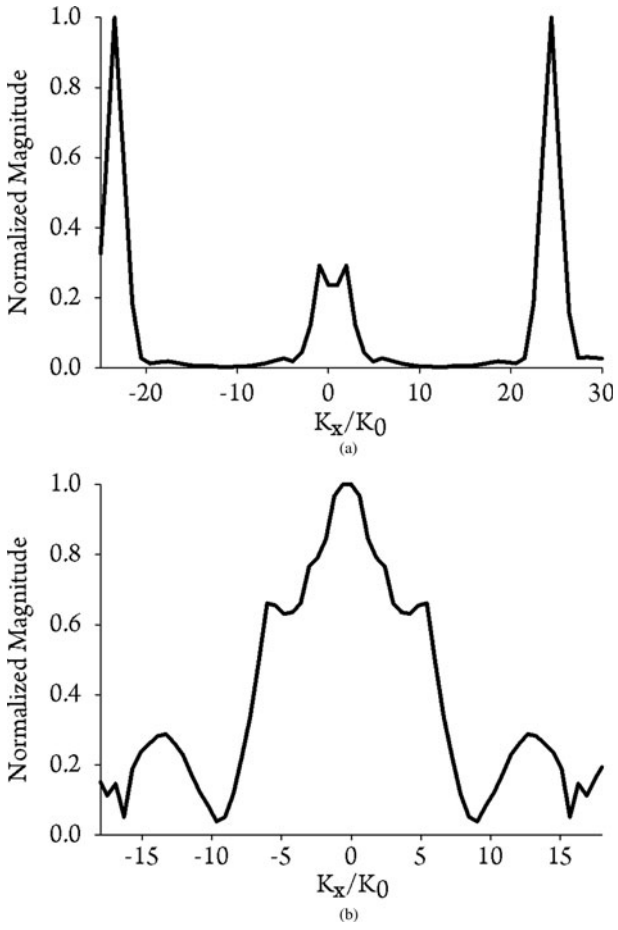

Fig. 8. Computed spatial frequency spectrum (a) free-standing dipole antenna and (b) metamaterial backed dipole antenna.

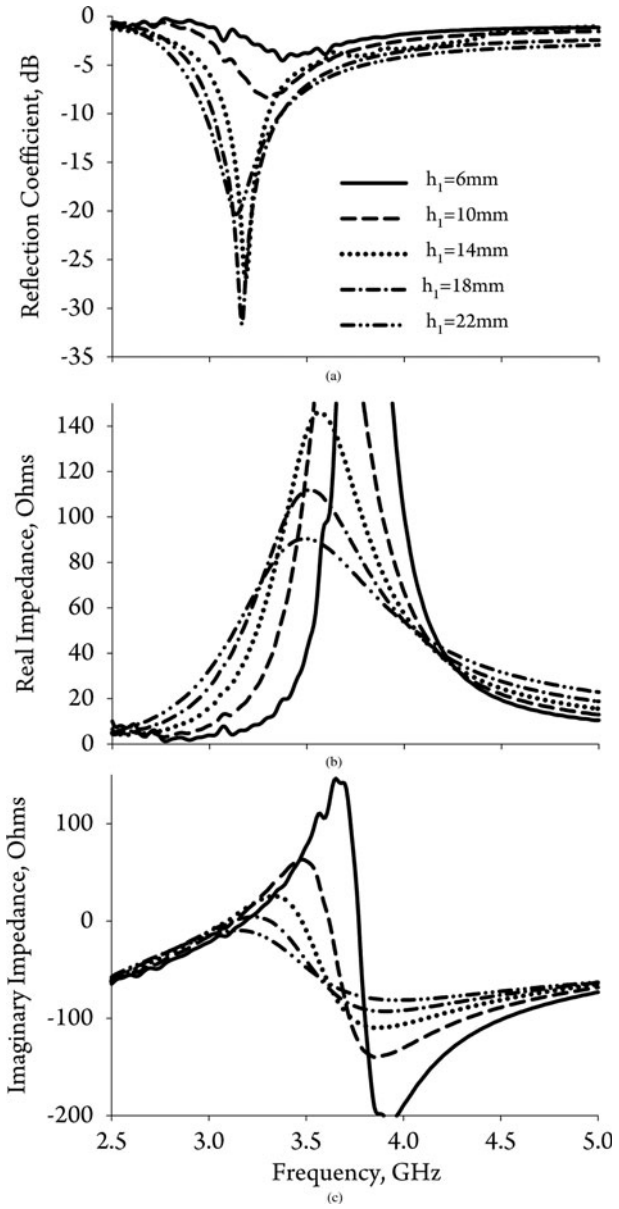

Fig. 9. Effect of loading height h_1 on antenna performance (a) variation in reflection coefficient, (b) variation real part of port impedance, and (c) variation imaginary part of port impedance.

radiation efficiency of the antennas. It is found that the free-standing balun loaded dipole shows an efficiency of 85% at resonance, whereas the absorber backed design shows an enhanced efficiency of the order of 98% due to spectral conversion.

A comparison study have been performed between the radiation performance of a conductor-backed dipole antenna and the metamaterial absorber-backed dipole configuration and the results are illustrated in Fig. 7. The metal plate on the back side of the antenna occupies the same area as that of the aperture area of the metamaterial absorber and the loading heights remains the same ($h_1 = 14$ mm). Figures 7(a) and 7(b) illustrates the 3D radiated gain patterns of the two configurations. The conductor backed dipole shows a gain of only 6.3 dBi along the broadside direction whereas the proposed design achieves a gain of 9.77 dBi at resonance. Figures 7(c) and 7(d) represent the comparison between *H*-plane and *E*-plane gain patterns of the two prototypes. It can be clearly seen that the absorber backed configuration significantly enhances radiation along the upper hemisphere proving its superior performance over conductor backed designs.

The theory behind gain enhancement can be easily understood by looking into the antenna near-field. The near-field contains some useful information about the radiation behavior of the antenna. It is well known that a dipole antenna contains both propagating as well as reactive fields within its near-field. The presence of both these components can be detected by taking the spatial Fourier Transform of the near-field electric field [21]. With the simulation software, it is easy to compute the electric field distributions on a plane. We have taken the spatial frequency distributions of the free-standing dipole antenna and the metamaterial absorber loaded dipole. The results are summarized in Fig. 8. Figure 8(a) shows the spatial frequency distribution of the simple dipole (without metamaterial). It is clear that the magnitude of the low-spatial frequency components corresponding to the propagating wave is comparatively low. The visible region is denoted with a region in which the ratio $|K_x/K_0| < 1$ and all other regions denote the invisible region. Invisible region contains reactive power and the visible region is responsible for far-field radiation. In the invisible region, there exists temporal phase difference between the electric and magnetic fields. The near-field of the dipole is dominated by the high-spatial frequency components designated as the reactive near-field. The presence of

the dominant reactive distributions severely affects the radiation performance of the antenna [22]. In our configuration, the metamaterial absorber in effect reflects the reactive power from the antenna and converts it into low spatial propagating components. In physical sense, this is equivalent to reducing the temporal phase difference electric and magnetic fields within the near-field of the antenna. Periodic perturbations in the near-field of the source is responsible for this conversion. In the case of an optical microscope, in order to achieve super resolution, periodic perturbations in the form of dielectric cylinders are introduced resulting in spectral conversion [23, 24]. In the case of absorber loaded design, spatial conversion occurred has been verified by checking the spatial-frequency spectrum as shown in Fig. 8(b). It is clear that placing the absorber in the vicinity of the dipole converts the reactive high-spatial frequency components into low spatial propagating components. The magnitude of propagating components is found to be greatly enhanced in comparison with the free-standing dipole.

Optimum loading height h_1 is selected after running a rigorous parametric analysis in CST Microwave Studio. The effect of variation in loading height on the reflection coefficient and input impedance characteristics are illustrated in Fig. 9. It is observed that when the dipole antenna is placed in close proximity with the absorber layer, the impedance matching performance is found to be deteriorated due to highly inductive reactance. Increasing the value of h_1 improves the impedance matching performance of the antenna and it is seen that increase in loading height severely decreases the imaginary part of port impedance thereby achieving resonant matching. It is also observed that increasing h_1 increases the 2:1 VSWR bandwidth of the antenna. The higher the loading height, the higher will be the bandwidth. For the three well-matched cases ($h_1 = 14$ mm, $h_1 = 18$ mm and $h_1 = 22$ mm), the gain and radiation efficiency remains almost constant and hence $h_1 = 14$ mm has been selected as the optimum design.

Conclusions

A dogbone metamaterial-based electromagnetic absorber is utilized for enhancing the radiation performance of a standard metal plate dipole antenna working in the S-band. The anomalous reflection of reactive high spatial near-field components from an artificial dielectric exhibiting strong imaginary part of permittivity is the cause of radiation enhancement. It is observed that the reactive near-field spectrum is converted into low spatial propagating spectrum above the antenna plane. The antenna attains highly collimated radiation patterns and the gain is enhanced to 10 dBi at resonance.

Acknowledgments. The authors acknowledge the financial support received from Department of Science and Technology (DST) and University Grants Commission (UGC), Government of India.

References

1. **Harvey AF** (1960) Periodic and Guiding structures at microwave frequencies. *IRE Transactions on Micowave Theory and Techniques* **1**, 30–61.
2. **Alu A, Engheta N, Erentok A and Ziolkowski RW** (2007) Single-Negative Double-Negative and low-index metamaterials and their electromagnetic applications. *IEEE Antennas and Propagation Magazine* **49**, 23–35.
3. **Engheta N and Ziolkowski R** (2006) *Metamaterials: Physics and Engineering Explorations*. New York: Wiley-IEEE Press.
4. **Monticone F, Estakhri NM and Alu A** (2013) Full control of nanoscale optical transmission with a composite metascreen. *Physical Review Letters* **110**, 203903.
5. **Pendry JB** (2000) Negative refraction makes a perfect lens. *Physical Review Letters* **85**, 0–3.
6. **Zhu BO, Zhao J and Feng Y** (2013) Active impedance metasurface with full 3600 reflection phase tuning. *Nature Scientific Reports* **49**, 1–6.
7. **Zhu BO, Chen K, Jia N, Sun L, Zhao J, Jiang T and Feng Y** (2014) Dynamic control of electromagnetic wave propagation with the equivalent principle inspired tunable metasurface. *Nature Scientific Reports* **4**, 1–7.
8. **Zhou J, Zhang L, Tuttle G, Koschny T and Soukoulis CM** (2006) Negative index materials using simple short wire pairs. *Physical Review B* **73**, 041101.
9. **Donzelli G, Vallecchi A, Capolino F and Schuchinsky A** (2009) Metamaterial made of paired planar conductors: Particle resonances phenomena and properties. *Metamaterials, Elsevier* **3**, 10–27.
10. **Capolino F** (2009) *Metamaterials Handbook-Theory and Phenomena of Metamaterials*. Boca Raton, CA: CRC Press, Taylor and Francis Group.
11. **Beruete M, Rodriguez-Ulibarri P, Pacheco-Pena V, Navarro-Cia M and Serebryannikov AE** (2013) Frozen mode from hybridized extraordinary transmission and Fabry-Perot resonances. *Physical Review B* **205128**, 1–9.
12. **Sarin VP, Pradeep A, Jayakrishnan MP, Chandroth A, Mohanan P and Kesavath V** (2016) Tailoring the spectral response of a dogbone doublet metamaterial. *Microwave and Optical Technology Letters* **58**, 1347–1353.
13. **Ra Y, Member S, Asadchy VS and Tretyakov SA** (2013) Total absorption of electromagnetic waves in ultimately Thin Layers. *IEEE Transactions on Antennas and Propagation* **61**, 4606–4614.
14. **Sullivan DM** (2013) Electromagnetic simulations using the FDTD method. Piscataway, NJ: Wiley-IEEE Press.
15. **De Moerloose J and Stuchly MA** (1995) Behavior of BerengerâĂŹ ABC for evanescent waves. *IEEE Microwave And Guided Wave Letters* **5**, 344–346.
16. **Valagiannopoulos CA and Tretyakov SA** (2016) Theoretical concepts of unlimited-power reflectors absorbers and emitters with Conjugately matched layers. *Physical Review B* **125117**, 1–13.
17. **Anantha Ramakrishna S, Armour AD and Ramakrishna SA** (2003) Propagating and evanescent waves in absorbing media. *American Journal of Physics* **71**, 562–567.
18. **Saenz E, Ederra I, Ikonen P, Tretyakov S and Gonzalo R** (2007) Power transmission enhancement by means of planar meta-surfaces. *Journal of Optics A: Pure and Applied Optics* **9**, 308–314.
19. **Choi J, Kim J and Jung C** (2013) Double-negative reconfigurable resonator with cross-polarised split rings. *Electronics Letters* **49**, 49–50.
20. **Wang H** (1997) Reflection of evanescent waves. *Revista Mexicana de Fisica* **6**, 916–925.
21. **Tamura M** (1990) Spatial Fourier transform method of measuring reflection coefficients at oblique incidence I: Theory and numerical examples. *The Journal of the Acoustical Society of America* **88**, 2259–2264.
22. **Valagiannopoulose CA and Alu A** (2015) The role of reactive energy in the radiation by a dipole antenna. *IEEE Transactions on Antennas and Propagation* **63**, 3736–3741.
23. **Pawliuk P and Yedlin M** (2014) Evanescent wave impedance and scattering conversion into radiation. *Applied Physics. B, Lasers and Optics* **114**, 407–413.
24. **Ben-Aryeh Y** (2008) Transmission enhancement by conversion of evanescent to propagating waves. *Applied Physics B Laser and Optics* **91**, 157–165.

Sarin Valiyaveettil Pushpakaran received his M.Sc degree in Applied Electronics in 2006 and Ph.D. degree in Microwave Electronics from Cochin University of Science and Technology, Kerala, India in 2012. He is currently an Assistant Professor in Department of Electronics, Government College Chittur, Palakkad, Kerala. His main research interests are Metamaterials, Wireless Power Transmission, Microwave Antennas and FDTD techniques.

Jayakrishnan M Purushothama received his B.Sc in Electronics from Aquinas College, Mahatma Gandhi University and M.Sc in Electronics Science in 2014 from Cochin University of Science and Technology, Kerala, India. His research interest includes microwave antennas, RFID tags and metamaterials.

Manoj Mani received his M.Sc in Electronics from Cochin University of Science and Technology, Kerala, India in 2015 and currently pursuing Ph.D. in Centre for Research in Electromagnetics and Antennas. He was awarded the Junior Research fellowship by University Grants Commission in 2014 and has been working at Cochin University of Science and Technology since 2015. His current research interests include Electrically Small Antennas, RFID tags and antennas for Biomedical applications.

Aanandan Chandroth was born in India. He received the M.Sc. and Ph.D. degrees from Cochin University of Science and Technology (CUSAT), Cochin, India, in 1981 and 1987, respectively. Currently, he is a Professor in the Department of Electronics, CUSAT. He is the coordinator for Advanced Centre for Atmospheric Radar Research (ACARR)funded by Department of Science and Technology (DST), Governement of India. From 1997 to 1998, he worked at the Centro Studi Propagazione E Antenne. Consiglio Nazionale Delle Ricerche, Torino, Italy, under the TRIL program of the International Centre for Theoretical Physics (ICTP). His research interests include microstrip antennas, radar cross section studies and frequency selective surfaces.

Mohanan Pezholil was born in India. He received the Ph.D. degree in microwave antennas from Cochin University of Science and Technology (CUSAT), Cochin, India, in 1985. Previously, he worked as an Engineer in the Antenna Research and Development Laboratory, Bharat Electronics, Ghaziabad, India. Currently he is an Emeritus Professor in the Department of Electronics, CUSAT. He is the co investigator for Advanced Centre for Atmospheric Radar Research (ACARR) project funded by Department of Science and Technology (DST), Governement of India. He has published more than 100 refereed journal papers and numerous conference articles. He also holds several patents in the areas of antennas and material science. His research areas include microstrip antennas, dielectric resonator antennas, superconducting microwave antennas, reduction of radar cross sections, and polarization agile antennas.

Vasudevan Kesavath was born in India. He received the M.Sc. degree in physics from Calicut University, Kerala, India and the Ph.D. degree from Cochin University, Cochin, India, in 1976 and 1982, respectively. From 1980 to 1984, he worked at St. Alberts College Ernakulam, Kerala, India. In 1985, he joined the Electronics Department of CUSAT where he is currently the Emeritus Professor. He is the co investigator for Advanced Centre for Atmospheric Radar Research (ACARR) project funded by Department of Science and Technology (DST), Governement of India. His research interests includes microstrip antennas, leaky wave antennas and radar cross section studies. Dr. Vasudevan is a Fellow of the Institution of Electronics and Telecommunication Engineers (India).

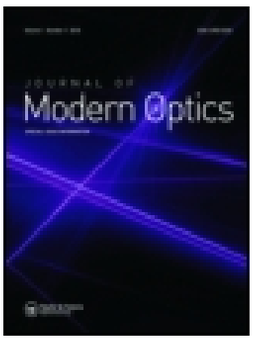

Journal of Modern Optics

ISSN: 0950-0340 (Print) 1362-3044 (Online) Journal homepage: http://www.tandfonline.com/loi/tmop20

Enhanced radiation from an electrically small radiator using an array of sub-wavelength holes

V. P. Sarin, Manoj Mani, Lindo Ouseph, Aanandan Chandroth, Mohanan Pezholil & Vasudevan Kesavath

To cite this article: V. P. Sarin, Manoj Mani, Lindo Ouseph, Aanandan Chandroth, Mohanan Pezholil & Vasudevan Kesavath (2018): Enhanced radiation from an electrically small radiator using an array of sub-wavelength holes, Journal of Modern Optics, DOI: 10.1080/09500340.2018.1512672

To link to this article: https://doi.org/10.1080/09500340.2018.1512672

Published online: 05 Sep 2018.

JOURNAL OF MODERN OPTICS
https://doi.org/10.1080/09500340.2018.1512672

Taylor & Francis
Taylor & Francis Group

Enhanced radiation from an electrically small radiator using an array of sub-wavelength holes

V. P. Sarin[a], Manoj Mani[b], Lindo Ouseph[b], Aanandan Chandroth[b], Mohanan Pezholil[b] and Vasudevan Kesavath[b]

[a]Department of Electronics, Government College Chittur, Kerala, India; [b]Department of Electronics, Centre for Research in Electromagnetics and Antennas, Cochin University of Science and Technology, Kerala, India

ABSTRACT

An experimental demonstration of radiation enhancement from an electrically small antenna (ESA) using an array of sub-wavelength holes engraved on a metallic plate is presented in this paper. A weakly radiating, chip inductor loaded open coplanar waveguide transmission line is used as the reference ESA. We show that an array of sub-wavelength hole loaded metallic aperture, placed near the antenna, can significantly enhance radiated power from the source. The hole array converts the high spatial reactive spectrum existing in the near-field of the antenna into a far-field propagating spectrum. The theory is validated by experiments and simulations in the microwave frequency regime. This novel radiation enhancement scheme is seen to enhance the gain of the antenna from −8.5 to −2.5−dBi and radiation efficiency from 13 to 33% around resonance.

ARTICLE HISTORY
Received 30 March 2018
Accepted 9 August 2018

KEYWORDS
Electrically small antennas; spectral conversion; sub-wavelength hole array

1. Introduction

The theory behind light transmission through a single sub-wavelength hole has been a great source of inspiration for electromagnetic research. The first successful theory behind this transmission was postulated by H. A. Bethe (*1*). The excitation of electric and magnetic dipole moments on the perforated metal screen is responsible for wave transmission through the hole. Following his invention, a variety of studies have been performed for enhancing wave transmission in the THz region beyond Bethe limit (*2*, *3*). In 1999, Ebbessen et al. showed that the transmission magnitude can be enhanced tremendously by perturbing the metal surface with a periodic array of sub-wavelength holes, resulting in extraordinary transmission (EOT) (*4*). D. R. Jackson and Oliner explained the EOT phenomenon using the leaky wave theory (*5*, *6*) and applied the concept for directional beam forming in antennas (*7*, *8*). Periodic perturbations are responsible for an infinite number of spatial harmonics and the $n = -1$ spatial one radiates along the broadside direction resulting in transmission enhancement. They concluded that the directive radiation pattern could be achieved by properly exciting a pair of transverse electric and transverse magnetic modes in an antenna structure. Sorolla et al. used the stacked perforated hole plates for enhancing wave transmission for antenna application in the millimetre and microwave frequency regime (*9*, *10*). Engheta et al. applied Epsilon Near Zero metamaterials as covers for a single sub-wavelength hole for enhancing transmission (*11*). The proposed theory has been experimentally validated in the microwave frequency range using transmission line Epsilon Near Negative Near Zero metamaterials (*12*). An array of sub-wavelength slit also shows EOT peaks in the microwave domain and the reason behind this resonant transmission is the excitation of Fabry–Perot resonant modes on the structure (*13*, *14*). Recently, the EOT transmission scheme has also been used for enhancing the front-to-back ratio of microwave antennas (*15*). The EOT scheme finds applications in enhanced spectroscopy and plasmonic-based chemical sensors (*16*). The lattice parameters and the shape of the hole could be optimized for a strong polarization-dependent resonant transmission scheme (*17*). The usage of graphene-based tunable EOT systems is well known among plasmonic research community (*18*–*20*).

In this study, another interesting property of an array of sub-wavelength circular holes engraved on a metallic sheet is utilized for enhancing the radiation characteristics of an electrically small antenna (ESA). It is observed that the array can convert the high spatial reactive near field radiated by an electrically small source into propagating spectrum. Classically, ESAs are characterized by a very high quality factor and its physical dimensions are described using the Chu limit (*21*). The normally used

CONTACT V. P. Sarin sarincrema@gmail.com Department of Electronics, Government College Chittur, Kerala 678104, India

terminology is that any antenna whose 'ka' value less than 0.5 can be termed as an ESA. Recently, a variety of research has been carried out on the design and development of ESAs (22–26). It is well known that an ESA has almost all its radiated energy concentrated in its reactive near field, which severely deteriorates its radiation efficiency. Ziolkowski and Kipple utilized artificial metamaterial inclusion around the ESA in order to match the highly capacitive reactance of the ESA with the inductance offered by the metamaterial, resulting in enhanced radiation performance (27). There are several theoretical and practical approaches of utilizing sub-wavelength gratings for converting the high spatial spectrum emitted by an evanescent source into far-field radiation (28, 29). Recently, metamaterial resonators have been effectively used for enhancing radiation from an electrically small split-ring antenna (30).

In this work, a sub-wavelength hole array engraved on a metallic plate is utilized for enhancing the radiation characteristics of an electrically small radiator in the S-band. The novelty of the proposed design is that it is devoid of conventional metamaterial inclusions in the form of artificial plasma layers (27) and magnetic resonators (30) for gain enhancement. Simulation studies of the antenna are done using the CST Microwave Studio and experiments are conducted using the Agilent PNAE8362B vector network analyzer. A comparison has been made between the radiation performance of the normal conductor backed antenna and the presented design to validate the predominance of the proposed concept.

2. Selection and characterization of the ESA source

2.1. Theory and geometry

The power radiated from an elementary electrically small dipole source is approximated as (17),

$$P = \eta\left(\frac{\pi}{3}\right)\left|\frac{I_0}{\lambda}l\right|\left[1 - j\frac{1}{(kr)^3}\right] \quad (1)$$

where η is the wave impedance, I_0 is the driving current, l is the length of the antenna, k is the wave number and λ is the operating wavelength. The above equation implies that the radiator has a capacitive near field, having reactance ratio lesser than unity. This highly capacitive reactive power limits the radiation efficiency of an ESA. Reactive power indicates that there exists a temporal phase shift between electric and magnetic fields radiated by the source. The reactive near field can be perturbed using periodic inclusions in the form of an array of sub-wavelength holes printed on a metallic sheet, resulting in enhanced radiation efficiency.

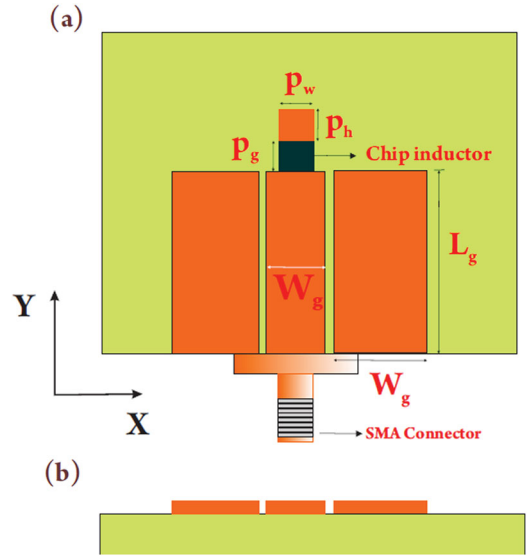

Figure 1. Geometric description of the reference electrically small antenna. (a) Top view and (b) side view.

For experimental realization, we have used the chip inductor loaded open coplanar waveguide as the reference antenna (31). The antenna occupies an area of $0.08\lambda_0 \times 0.0479\lambda_0$ and at the resonant frequency, the *ka* value is 0.2924, which is much smaller than the Chu limit. The proposed ESA configuration is depicted in Figure 1. The antenna comprises of a simple Open Coplanar Waveguide with one end of the centre conductor soldered with a chip inductor of 23 nH on to the top base metallization. Microwave signal is fed using a standard SubMiniature version A (SMA) connector soldered to the lower bottom end of the Coplanar Waveguide as shown. The dimensions of the antenna are $P_g = 0.8$ mm, $P_w = 1$ mm, $P_h = 0.8$ mm, $L_g = 4$ mm, and $W_g = 3$ mm. The antenna is fabricated on a low-cost Copper cladded epoxy substrate of dielectric constant 4.4 and thickness h = 1.6 mm using photo-lithography.

2.2. Results and discussions

The CST Microwave Studio computational platform utilizes the finite integration technique to discretize the integral form of Maxwell's equations (32). Time domain solver, utilizing the Leap-Frog algorithm, is used to calculate the electromagnetic fields within the computational domain. In the simulation, a waveguide port is assigned on the input face of the SMA connector and a standard time domain Gaussian pulse is used as the excitation. By calculating the ratio between the reflected and input time domain signals and application of discrete Fourier transform yields the reflection coefficient of the antenna. The

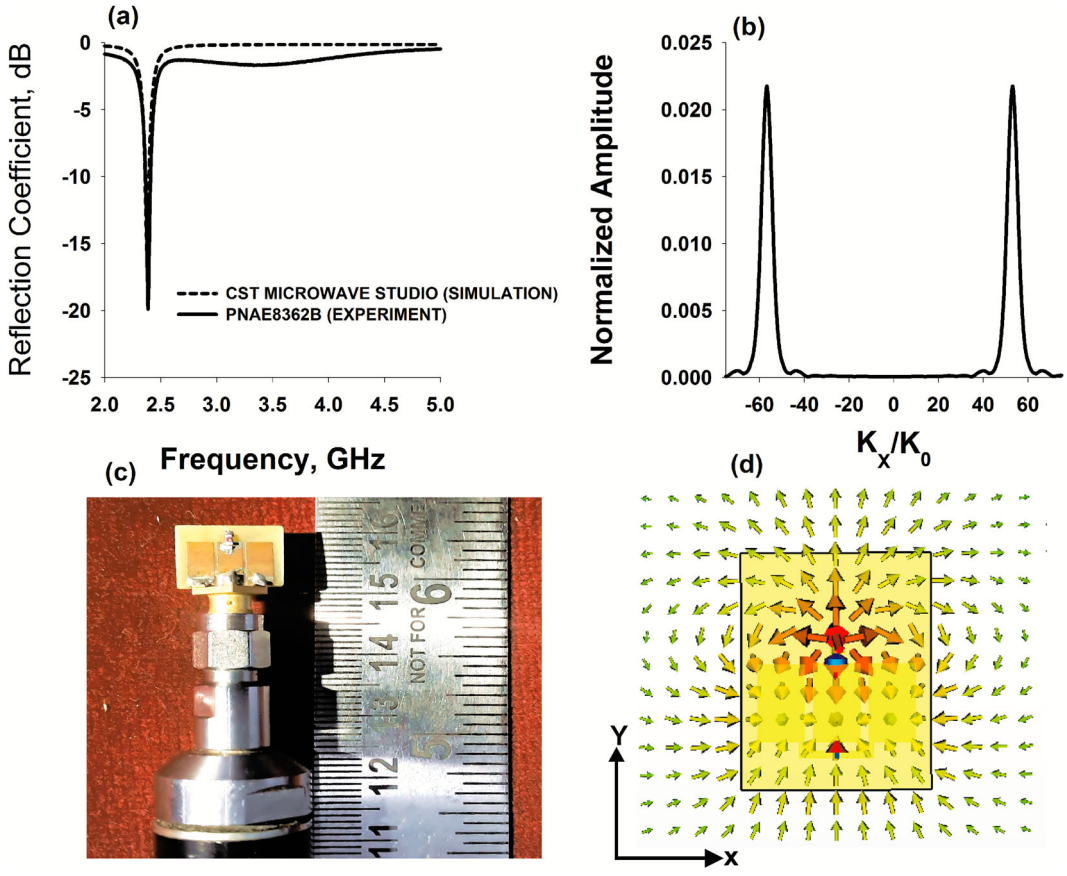

Figure 2. Characterization of the reference ESA. (a) Measured and simulated reflection coefficient, (b) spatial spectrum radiated by the antenna, (c) photograph of the fabricated antenna, and (d) simulated electric field distributions on the antenna aperture.

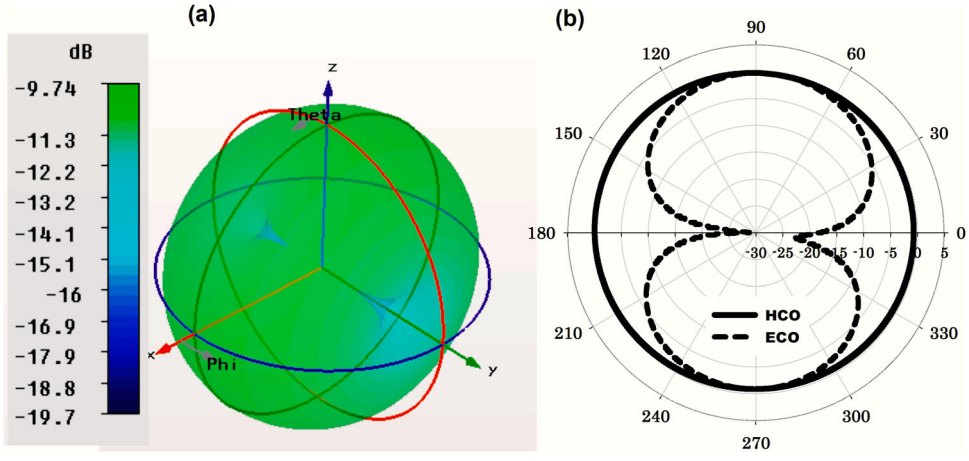

Figure 3. Radiation characteristics of the reference ESA. (a) Simulated 3D radiation pattern at resonance and (b) E-plane and H-plane co-polar patterns.

reflection and radiation characteristics of the reference ESA are given in Figures 2 and 3, respectively. The measured and simulated reflection characteristics of the ESA are depicted in Figure 2(a).

The antenna resonates at 2.37 GHz with a reflection coefficient of −20 dB. The 2:1 VSWR bandwidth (|S11| < −10 dB) is 2% around the resonant frequency. The measured gain of the antenna is only −8.5 dBi at resonance, and hence this ESA could not be considered as an efficient radiator. The radiation efficiency, measured using the Wheeler-Cap method, is found to be only 13% at resonance. The reason for poor radiation efficiency could be well understood by looking into the spatial Fourier transform of the antenna near field. The

normalized spatial frequency spectrum radiated by the ESA is shown in Figure 2(b). The Fourier components having spectral components $|K_X/K_0| > 1$ is denoted as the invisible spectrum and the spectra with $|K_X/K_0| < 1$ is termed as the visible spectrum. The visible low spatial spectrum is responsible for far-field radiation and the invisible spectrum contributes reactive power within the near field of the ESA. One could see that the antenna near field is dominated by the invisible spectrum and the propagating spectrum is inevitably small resulting in low radiation efficiency. The photograph of the fabricated ESA is shown in Figure 2(c). The resonant mechanism can be easily understood by studying the near-field electric field distribution on the antenna structure depicted in Figure 2(d). Resonance is attributed due to the monopole excitation on the antenna structure. The out-of-phase E_x components of electric fields on the left and right sides of the antenna cancel each other at the far-field and radiation is attributed due to the in-phase E_y components. Hence, polarization of the antenna is lying along the Y-axis.

The simulated 3D radiation pattern of the antenna at resonance is shown in Figure 3(a). The antenna shows omni-directional radiation pattern and the polarization is directed along the Y-axis. The E-plane and H-plane co-polar patterns at resonance are illustrated in Figure 3(b). The cross polar isolation is −15 dB for the E-plane and −13 dB for the H-plane.

3. The sub-wavelength hole array backed ESA

3.1. Geometrical specifications

When the ESA is brought in the vicinity of a sub-wavelength hole array, it is observed that the radiation performance of the antenna is enhanced. The geometry of the loaded antenna configuration is shown in Figure 4. The sub-wavelength circular hole array lies in the XY plane of the coordinate system. Radius (r) of the hole is optimized as 0.5 mm and the lattice constant (a) is 2 mm. The simulated and fabricated structure has a total of 144 holes arranged as a 12 × 12 array. The copper metallization has a thickness of 35 μm and occupies an area of 60 × 60 mm^2 when printed on an epoxy substrate of dielectric constant 4.4 and thickness 1.6 mm. The 0.5 mm hole implies that the Wood anomaly resonance is expected to occur at a higher frequency band compared to the S-band frequencies and hence the fields existing inside the holes will be evanescent for the band of interest (*33*). For simulation, the metal plate is treated as perfect electric conductor (PEC) and the standard Drude-dispersion model is not fitted with CST simulation. This is due to the fact that Copper plate at microwave frequencies acts like a perfect reflector and the Drude model is required only at near-infrared and optical frequencies (*34*). For a normally incident plane wave, the transmission magnitude will be negligibly small for this array. This holds true only for propagating transverse electromagnetic waves. In the case of an ESA, the near field contains reactive power and it is observed that when such an antenna is placed near the hole array, the radiation efficiency of the radiator could be significantly enhanced.

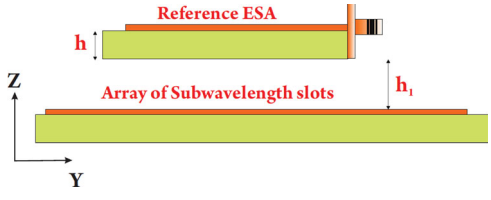

Figure 4. Geometry of the sub-wavelength hole loaded metallic plate backed antenna.

3.2. Results and discussions

3.2.1. Parametric variations

The loading height h_1 is optimized after running rigorous parametric simulations in the CST Microwave Studio. The variation in radiation characteristics of the antenna for different loading heights is depicted in Figure 5. It is observed that the impedance matching characteristics of the antenna remains unaltered by varying the loading height, whereas the variation severely affects the radiated power from the antenna. Figure 5(a) and (b) illustrates the effect of variation in h_1 on H-plane and E-plane radiation patterns. It is clear that increase in loading thickness gradually enhances radiated power from the antenna. Optimum design is selected to have a maximum gain and radiation efficiency. The simulated variation in efficiency and gain of the antenna against h_1 is shown in Figure 5(c). For a lower loading thickness ($h_1 = 5$ mm), the gain is found to be −8.2 dBi and correspondingly the radiation efficiency is 2.7%. The optimum design shows a maximum gain of −2.47 dBi and efficiency of 30% at resonance.

For measuring radiation patterns, an ultra wideband horn antenna is used as the receiving antenna and the received power is used for making the THRU calibration in the network analyzer. The antenna under test is rotated using a computer-controlled stepper motor assembly and the power received by the horn antenna is recorded for the principal planes. The measured variation in radiation patterns for the two principal planes against loading height is depicted in Figure 6(a) and (b) and show fairly good agreement with the simulation results. The effect of loading height on the reflection characteristics of the

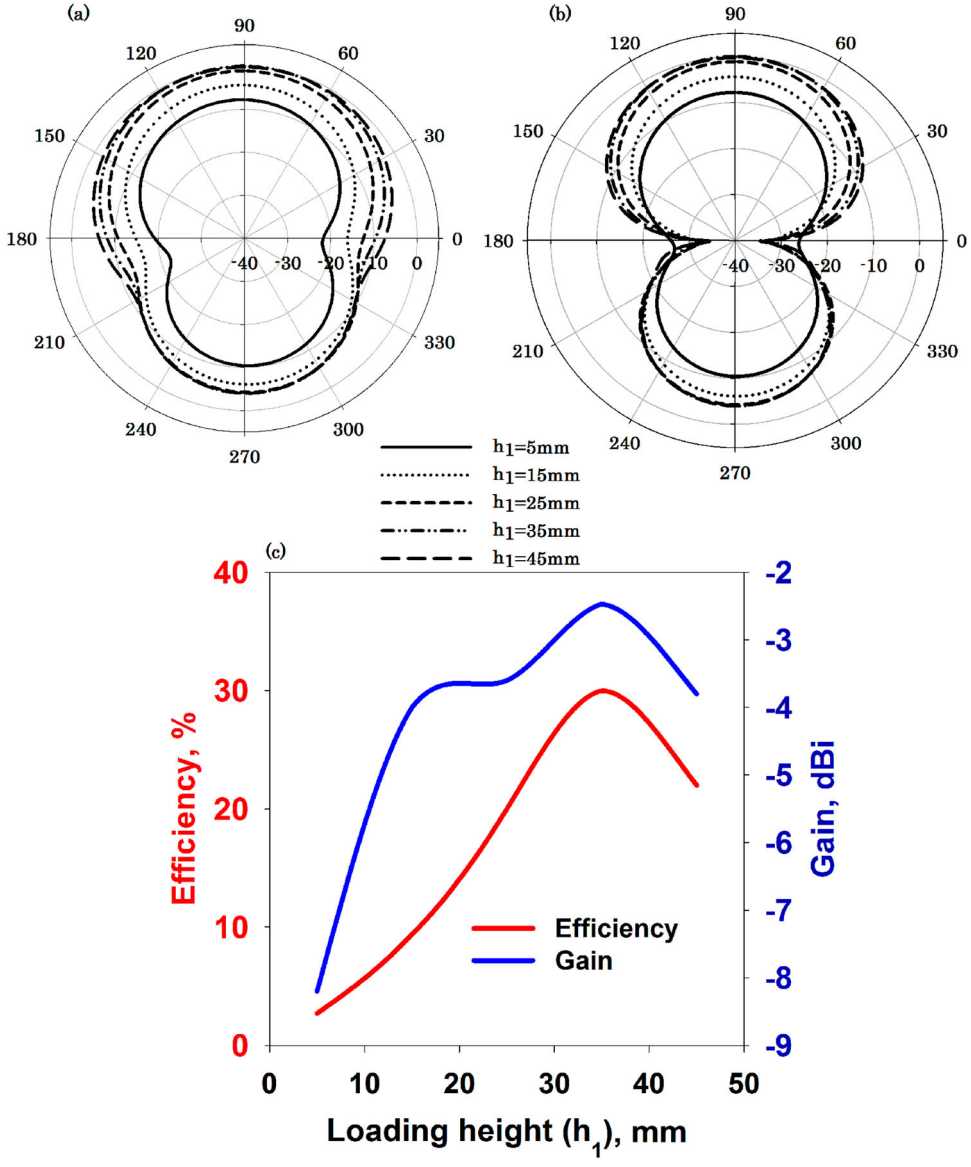

Figure 5. Effect of variation in loading height on radiation characteristics. (a) Variation in H-plane pattern, (b) variation in E-plane pattern and (c) dependence of radiated gain and efficiency on h_1.

antenna is depicted in Figure 6(c). It is noted that the resonant frequency remains unaltered for all the variations. Radiation efficiency is measured using the well-known Wheeler-Cap method. The variation of measured gain and efficiency, illustrated in Figure 6(d), also shows fair agreement with the simulation results. In experiments, the recorded gain is found to be −2.52 dBi for the optimum design and correspondingly, the radiation efficiency is 33% at resonance.

A comparison study has been performed between the proposed sub-wavelength hole array loaded ESA and a plane PEC backed ESA. The PEC conductor occupies the same area as that of the metal hole array. The effect of variation in gain and radiation efficiency of the conductor backed configuration is also given in Figure 6(d). It is observed that the PEC backed design shows a maximum gain of only −5 dBi at $h_1 = 45$ mm and the radiation efficiency is found to be only 8.4%. The PEC loaded configuration shows the minimum radiated gain, as the propagating low spatial components from the antenna are experiencing anti-phase reflection from the plate, resulting in destructive interference along the upper hemisphere of the computational domain.

The effect of hole radius and lattice constant on the radiation performance are also studied using CST simulations. The corresponding effect of variation in the E-plane and H-plane radiation patterns is illustrated in Figure 7. The parametric variations are performed by making the aperture area of the metallic plate and the loading height ($h_1 = 35$ mm) as constants. Three different

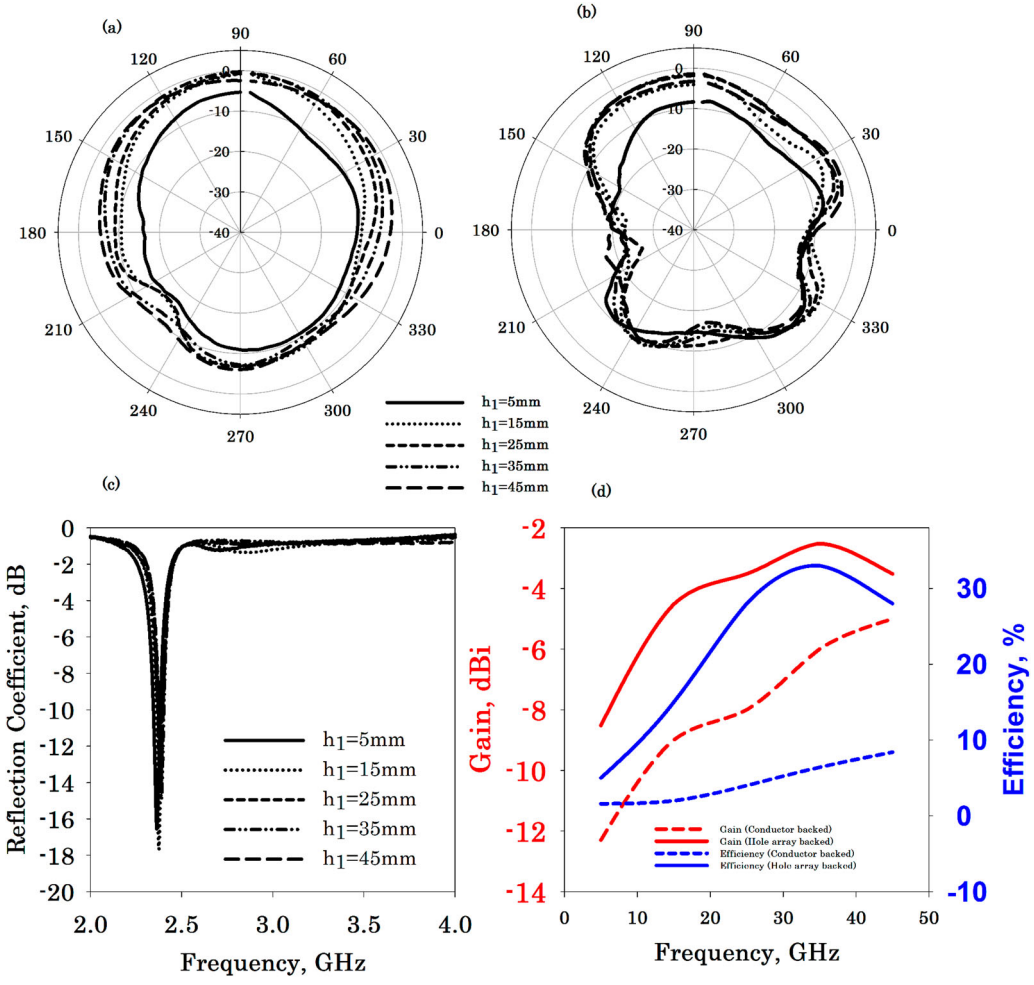

Figure 6. Effect of loading height on radiation patterns. (a) Variation in H-plane pattern and (b) variation in E-plane pattern.

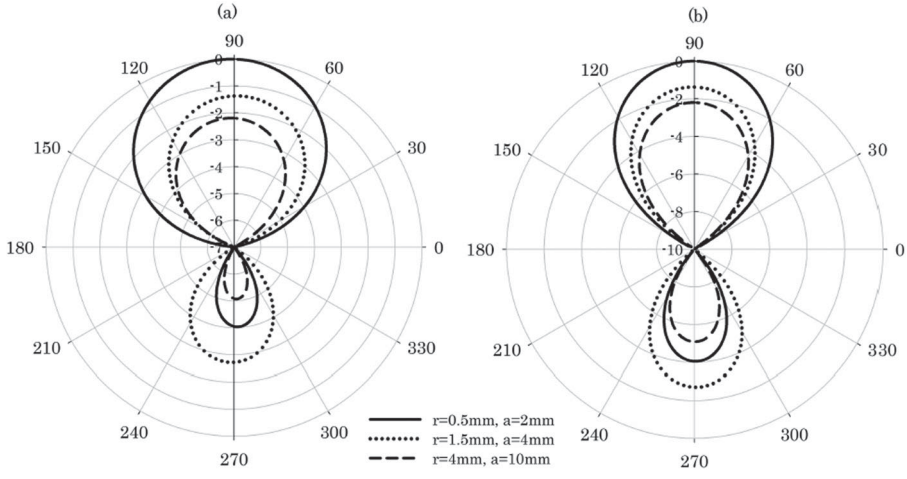

Figure 7. Effect of hole radius and lattice constant on radiation characteristics. (a) Variation in H-plane pattern, and (b) Variation in E-plane pattern.

prototypes are tested: one with $r = 0.5$ mm and $a = 2$ mm, the second with $r = 1.5$ mm and $a = 4$ mm and the third with $r = 4$ mm and $a = 10$ mm. It is obvious that decreasing the hole size enhances the radiated power along the broadside direction and hence the design with $r = 0.5$ mm and $a = 2$ mm has been selected as the optimum design. It is to be noted that the radiation efficiency and gain can be further enhanced by using deep sub-wavelength array of patterned holes. But due to the practical difficulty associated with the current

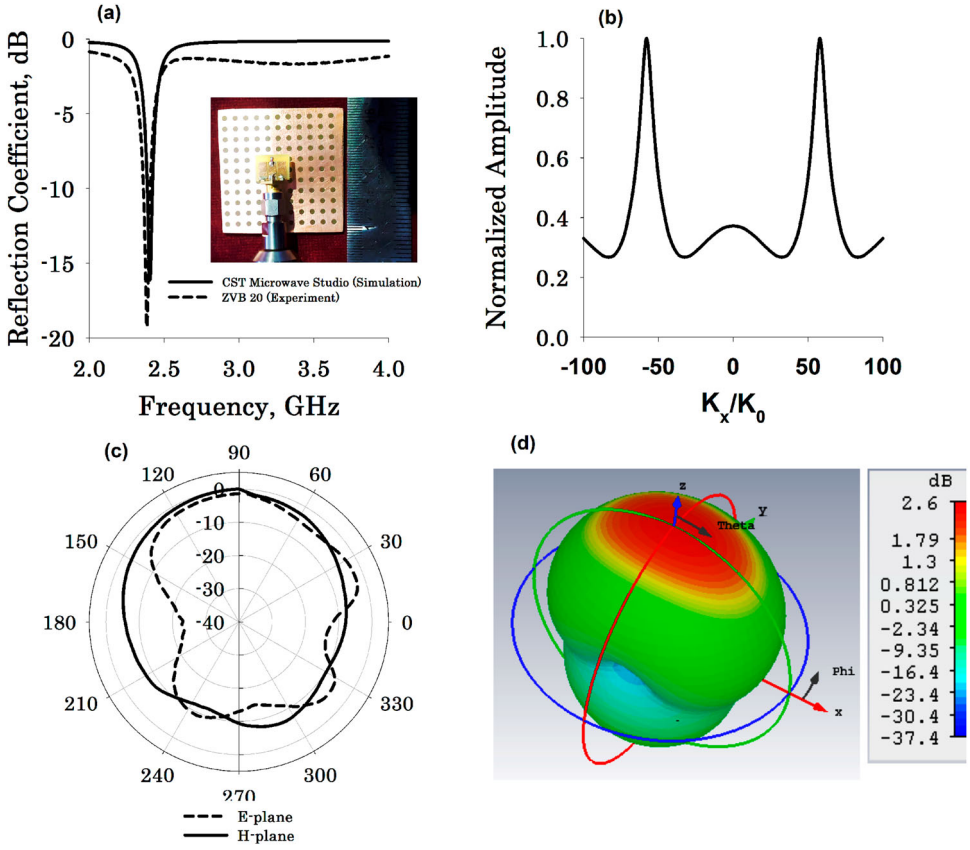

Figure 8. Characterization of the final antenna. (a) Measured and simulated reflection coefficients with photograph in the inset, (b) spatial frequency spectrum, (c) measured E-plane and H-plane radiation patterns, and (d) simulated 3D radiation pattern at resonance.

photo-lithographic fabrication, the array with $r = 0.5$ mm and $a = 2$ mm is selected as the optimum design.

3.2.2. The optimum design

The reflection and radiation characteristics of the optimum design are summarized in Figure 8. Figure 8(a) shows the reflection characteristics of the antenna. The experiment and simulation shows fairly good agreement with each other. It is observed that the antenna resonance remains the same as that of the unloaded case and 2:1 VSWR bandwidth is found to be 500 MHz at resonance. The spatial frequency spectrum computed from the near-field electric field distributions is summarized in Figure 8(b). It is seen that the spatial spectrum contains significant low spatial components as compared to the unloaded case. This indicates that the placement of sub-wavelength hole array near the antenna, efficiently converts the high spatial frequency into low spatial propagating components. Significant spectral spreading towards the propagating side ($|K_X/K_0| < 1$) is observed as compared to the unloaded case. The photograph of the fabricated prototype is shown in the inset of Figure 8(a). The measured E-plane and H-plane radiation patterns are plotted in Figure 8(c). The front-to-back ratio is found to be −8.9 dB at resonance. The simulated 3D radiation pattern of the antenna at resonance is shown in Figure 8(d). As expected, the loaded configuration shows directional radiation characteristics. Gain of the antenna, measured using the gain comparison method, is −2.5 dBi at the resonant frequency and correspondingly the efficiency is 33%.

4. Conclusions

An experimental realization of sub-wavelength hole array-based spectral conversion for enhancing the radiation performance of an ESA is demonstrated. A comparison study is presented between the performance of a conductor backed ESA and the slot array backed ESA and superiority of the proposed design is validated. Gain of the optimum design is enhanced to −2.5 dBi and the corresponding radiation efficiency is enhanced to 33%. The proposed design is simple, low cost and is devoid of conventional metamaterial structures for evanescent to propagation conversion.

Acknowledgements

The authors are thankful to Dr Mohammmed Memarian, Shariff Institute of Technology, Tehran, for his valuable technical advice.

Disclosure statement

No potential conflict of interest was reported by the authors.

Funding

The authors greatly acknowledge the research support received from Department of Science and Technology (DST), New Delhi and University Grants Commission (UGC), Government of India for research support.

References

(1) Bethe, H.A. Theory of Diffraction by Small Holes. *Phys. Rev. Lett.*. **1944,** *66*, 163.
(2) Ghaemi, H.F.; Thio, T.; Grupp, D.E. Surface Plasmons Enhance Optical Transmission Through sub-Wavelength Holes. *Phys. Rev. B.* **1998,** *58*, 6779.
(3) Scorrano, L.; Bilotti, F.; Member, S.; Vegni, L. Achieving Power Transmission Enhancement by Using Nano-Rings Made of Silver Spheres. *IEEE Photonics Tech. Lett.* **2010,** *21*, 1595.
(4) Ebbessen, T.A.; Lezec, H.J.; Ghaemi, H.F.; Thio, T.; Wolff, P.A. Extraordinary Optical Transmission Through sub-Wavelength Hole Arrays. *Nature Lett.* **1998,** *391*, 667.
(5) Lovat, G.; Ieee, M.; Capolino, F.; M, S. The Fundamental Physics of Directive Beaming at Microwave and Optical Frequencies and the Role of Leaky Waves. *Proc. IEEE.* **2011,** *99*, 1780.
(6) Jackson, D.R.; Chen, J.; Qiang, R.; Capolino, F.; Oliner, A.A. The Role of Leaky Plasmon Waves in the Directive Beaming of Light Through a sub-Wavelength Aperture. *Opt. Exp.* **2008,** *16*, 328.
(7) Burghignoli, P.; Member, S.; Lovat, G.; Capolino, F.; Member, S.; Jackson, D.R.; Wilton, D.R. Directive Leaky-Wave Radiation From a Dipole Source in a Wire-Medium Slab. *IEEE Trans. Ant. Propag.* **2008,** *56*, 1329.
(8) Lovat, G.; Burghignoli, P.; Jackson, D.R. Fundamental Properties and Optimization of Broadside Radiation From Uniform Leaky-Wave Antennas. *IEEE Trans. Ant. Propag.* **2006,** *54*, 1442.
(9) Beruete, M.; Campillo, I.; Navarro-cía, M.; Falcone, F.; Ayza, M.S. Molding Left or Right-Handed Metamaterials by Stacked Cutoff Metallic Hole Arrays. *IEEE Trans. Ant. Propag.* **2007,** *55*, 1514.
(10) Beruete, M.; Campillo, I.; Perea, E.; Sorolla, M. Enhanced Gain by Double-Periodic Stacked Subwavelength Hole Array. *IEEE Microwave Wireless Comp. Lett.* **2012,** *60*, 3893.
(11) Alù, A.; Bilotti, F.; Engheta, N.; Vegni, L. Metamaterial Covers Over a Small Aperture. *IEEE Trans. Ant. Propag.* **2006,** *54*, 1632.
(12) Baladi, E.; Pollock, J.G.; Iyer, A.K. New Approach for Extraordinary Transmission Through an Array of sub-Wavelength Apertures Using Thin ENNZ Metamaterial Liners. *Opt. Exp.* **2015,** *23*, 20356.
(13) Went, H.E.; Hibbins, A.P.; Sambles, J.R.; Lawrence, C.R.; Crick, A.P. Selective Transmission Through Very Deep Zero-Order Metallic Gratings at Microwave Frequencies. *Applied Physics Letters* **2000,** *77*, 2789.
(14) Hibbins, A.P.; Lockyear, M.J.; Sambles, J.R. The Resonant Electromagnetic Fields of an Array of Metallic Slits Acting as Fabry-Perot Cavities. Journal of Appl. *Physicist* **2006,** *99*, 124903.
(15) Sarin, V.P.; Jayakrishnan, M.P.; Aanandan, C.K.; Mohanan, P.; Vasudevan, K. Extraordinary Transmission Technique for Microwave Antenna Applications. *J. Phys. D: Appl. Phys.* **2016,** *49*, 185503.
(16) Gordon, R.; Sinton, D.; Kavanagh, K.L.; Brolo, A.G. New Generation of Sensors Based on Extraordinary Optical Transmission. *Acc. Chem. Res.* **2008,** *41*, 1049.
(17) Gordon, R.; Brolo, A.G.; McKinnon, A.; Rajora, A.; Leathem, B.; Kavanagh, K.L. Strong Polarization in the Optical Transmission Through Elliptical Nanohole Arrays. *Phys. Rev. Lett* **2004,** *92*, 037401.
(18) He, X.; Pingqi Gaob, A.; Shia, W. A Further Comparison of Graphene and Thin Metal Layers for Plasmonics. *Nanoscale* **2016,** *8*, 10388.
(19) He, X.; Lu, H. Graphene-Supported Tunable Extraordinary Transmission. *Nanotech* **2014,** *25*, 325201.
(20) He, X.; Liu, F.; Lin, F.; Shi, W. Graphene Patterns Supported Terahertz Tunable Plasmon Induced Transparency. *Opt. Exp.* **2018,** *26*, 9931.
(21) Chu, L.J. Physical Limitation of Omni-Directional Antennas. *J. Appl. Phys.* **1948,** *19*, 1163.
(22) Alu, A.; Bilotti, F.; Engheta, N.; Vengi, L. Sub-Wavelength, Compact Resonant Patch Antennas Loaded with Metamaterials. *IEEE Trans. Ant. aPropag.* **2007**, *55*, 13.
(23) Antoniades, M.; Eleftheriades, G. Folded-monopole Model for Electrically Small NRI-TL Metamaterial Antennas. *IEEE Trans. Ant. Wireless Propag. Lett.* **2006,** *5*, 483.
(24) Iizuka, H. Dipole Antenna with Left-Handed Loading. *IEEE Trans. Ant. Wireless Propag. Lett.* **2008,** *7*, 425.
(25) Stuart, H.R.; Pidwerbetsky, A. Electrically Small Antenna Elements Using Negative Permittivity Resonators. *IEEE Trans. Ant. Propag.* **2006,** *54*, 1644.
(26) Ziolkowski, R.W.; Erentok, A. At and Below the Chu Limit: Passive and Active Broad Bandwidth Metamaterial-Based Electrically Small Antennas. *IET Microwave Ant. Propag.* **2007,** *1*, 116.
(27) Ziolkowski, R.W.; Kipple, A.D. Reciprocity Between the Effects of Resonant Scattering and Enhanced Radiated Power by Electrically Small Antennas in the Presence of Nested Metamaterial Shells. *Phys. Rev. E* **2005,** *72*, 1.
(28) Memarian, M.; Eleftheriades, G.V. Evanescent–to-Propagating Wave Conversion in sub-Wavelength Metal Strip Gratings. *IEEE Trans. Microwave Theory Techn.* **2012,** *60*, 3893.
(29) Memarian, M.; Eleftheriades, G.V. Enhanced Radiation of an Invisible Array of Sources Through a sub-Wavelength Metal-Strip Grating and Applications. *J. Appl. Phys.*. **2014,** *114*, 134902.

(30) Peng, L.; Chen, P.; Wu, A.; Wang, G. Efficient Radiation by Electrically Small Antennas Made of Coupled Split-Ring Resonators. *Sci. Rep.* **2016,** *6*, 33501.
(31) Deepak, U.; Roshna, T.K.; Nijas, C.M.; Mohanan, P. Compact CPW Fed Electrically Small Antenna for WLAN Application. *IET Electr. Lett.* **2014,** *50*, 12.
(32) CST Design Studio [online]. Available: www.cst.com
(33) Hou, B.; Hang, Z.H.; Wen, W.; Chan, C.T.; Sheng, P. Microwave Transmission Through Metallic Hole Arrays: Surface Electric Field Measurements. *Appl. Phys. Lett.* **2006,** *89*, 131917.
(34) El-Kady, I.; Sigalas, M.M.; Biswas, R.; Ho, K.M.; Soukoulis, C.M. Metallic Photonic Crystals at Optical Wavelengths. *Phys. Rev. B* **2000,** *62*, 15299.

International Journal of Engineering and Techniques - Volume 4 Issue 2, April-2018

RESEARCH ARTICLE OPEN ACCESS

CONVOLUTION CODE FOR BETTER PERFORMANCE OF ULTRA LOW POWER TRANSCEIVER

S.Sindhu[1], A. Balamurugan[2]

1. *Assistant Professor, Dept. of Electronics, Govt. College Chittur, Palakkad-678104, Kerala, India.*
2. *Assistant Professor, Dept. of Physics, Govt. Arts College, Ooty-643002, Tamil Nadu, India*

Abstract:

This paper proposes, convolution code for better performance of ultra low power transceiver comparing to Hamming code. It targets ultra low power consumption; with reliable Quality of Service (QoS). Low complex architecture is provided here with Application Specific Integrated Circuit (ASIC) which satisfies a good performance. Better packet synchronization and data recovery is helpful for the satisfactory functioning of the ultra low power transceiver. With a 1.1V supply and 4MHz system clock the base band transceiver can decrease the power up to 7mW.

Keywords — **Wireless Body Area Network (WBAN), Transceiver, Convolution code, Power consumption.**

I. INTRODUCTION

Wireless Body Area Networks healthcare surveillance and monitoring devices

CLOCK GATING FOR ULTRA LOW POWER TRANSCEIVER

S. Sindhu ,

Assistant Professor, Dept. of Electronics, Govt. College Chittur, Palakkad-678104, Kerala, India.
sindhusiva1984@gmail.com

A. Balamurugan
[1.] *Assistant Professor, Dept. of Physics, Govt. Arts and Science College, Avinasi-641654, Tamil Nadu, India*
bala.snr@gmail.com

***Abstract*-Clock gating is a popular technique which can be used in different logic circuits for saving the power. It helps to reduce the power dissipation. It reduces the power consumption by adding more logic circuits. It disables the circuitry when the flip flops in the circuits need not change the states. The switching power consumption is zero, when the state is not needed to change. Only leakage current occurs. This paper proposes the Look-Ahead Clock Gating (LACG) for the ultralow power transceiver. This helps to decrease the total power used by the transceiver.**

Keywords: *Clock gating, ultra low power transceiver, Look-Ahead Clock Gating, Auto Gated Flip Flop.*

I. INTRODUCTION

Clock is the fundamental signal in any logic circuits. In earlier days no one was ready to manipulate the clock signal and provided to the logic circuit as clean as possible. Clock power plays a major role in the design of logic circuit. Recently it was realized that clock signal was a major part of the total power due to the signal in the digital circuits and also by the unnecessary switching activities by the clock. Clock consumes 60-70% of the total power. This is due to the fact that power is directly proportional to the voltage and frequency of the clock [1]. This is shown by the equation that,

$$P= CV^2f.$$

Today customer demands more energy efficient devices and optimized power devices. This can be achieved by switch off the clock of logic circuits when there is no function is required from that part at that time. So reducing clock power is much important. Clock gating is the simple technique used by the designers to control the power in the sequential logic circuits. By using this technique the designer can shut off the clock of certain parts of sequential logic circuit when there is no clock is needed. By this technique logic circuit can avoid the unwanted switching. The clock gating is developed specifically for the flip-flops. It helps to disable the clock when the input data does not change the stored data.

In the basic clock gating technique, AND gate is used to control the clock [1-3]. By ANDing the clock and gate control signal, the clock gating essentially disables the clock to the circuit, whenever the circuit is not used [4]. It helps to avoid the power dissipation due to unnecessary charging and discharging of the unused circuits. The Fig.1 shows a latch element, when the clock switches in every cycle, the capacitor C_g charges and discharges and consumes significant amount of power. When the input do not change from one clock to next clock, the latch still use the clock power.

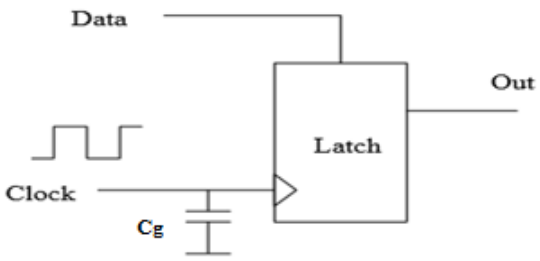

Fig. 1 A basic latch element without clock gating

The clock is controlled by ANDing it with a control signal Clk-gate signal, which is shown in Fig.2. When the latch is not needed to change the state, the clock signal is turned off and clock is not allowed to charge or discharge the C_g, saving the clock power.

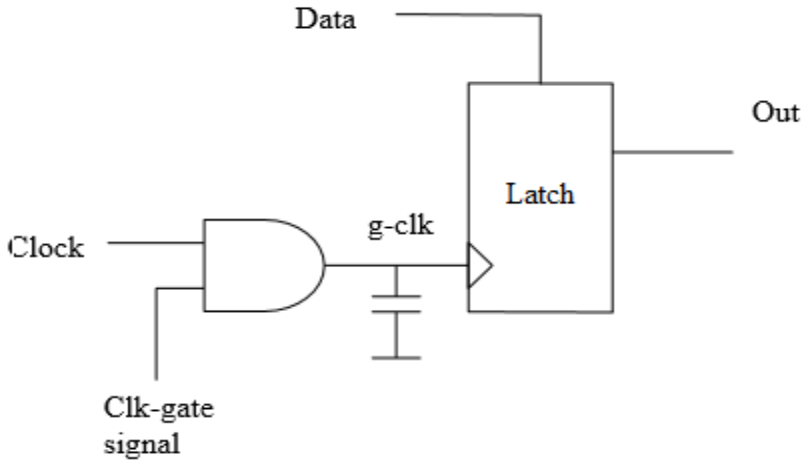

Fig. 2 Latch element with clock gating

A. Techniques for clock Gating:

There are four different techniques are available for the clock gating [1]. They are

1. Latch free based design.

2. Latch based design.

3. Flip-flop based design.

4. Intelligent clock gating.

1. Latch Free based design:

This one is the simplest technique. This uses the "AND" or "OR" gate for the clock gating in the sequential circuit, which is shown in Fig.3. The sequential circuit that operate on negative edge of the clock uses the AND gate. The circuit that operate on the positive edge of the clock uses the OR gate. Glitches may occur if clock gating is not done properly.

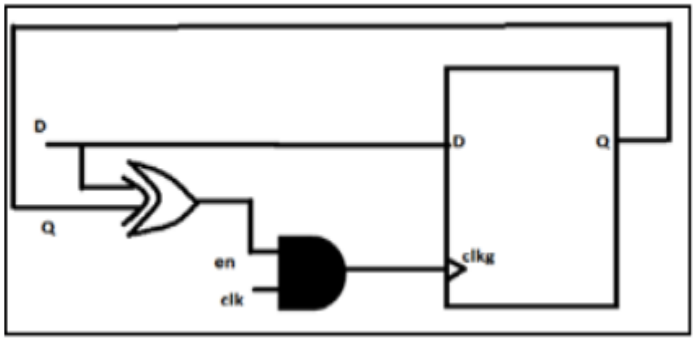

Fig. 3 Negative edge D Flip-Flop (Latch free based design)

2. Latch based design

A level sensitive latch is used as control element[1]. The output is used to control the enable pin, that is fed to the "AND" or "OR" gate for gating the circuit, which is shown in Fig.4. The latch helps to keep the value of the enable signal from positive edge of the clock to the negative edge of the clock. This circuit avoids the problem of the glitch.

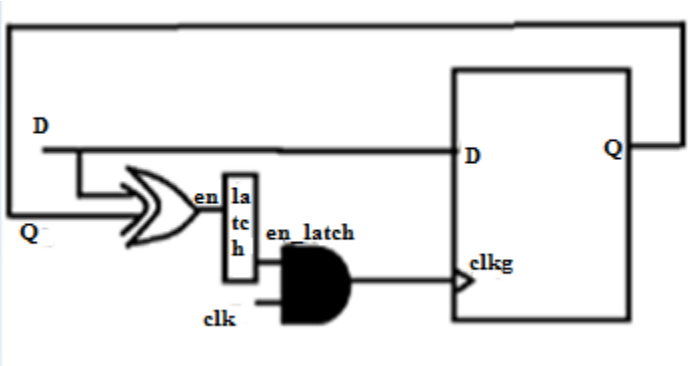

Fig.4 Negative edge D Flip-Flop (Latch based design)

3 .Flip –Flop based design

A flip-flop based design is similar to latch based design[1]. The basic difference is instead of level sensitive latch, an edge triggered flip-flop is used to control the enable signal. That is shown in Fig.5.

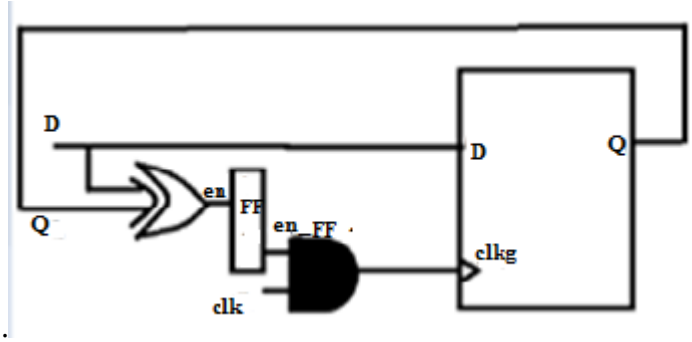

Fig. 5 Negative edge triggered D Flip-Flop (Flip-flop based design)

4. Intelligent Clock gating

A well programmed set of algorithms that can detect the unnecessary switching in the design and supress it[1]. This method help to add some logic to suppress and minimize the unessential activity in the function, which reduce the power consumption.

Three types of gating methods are used in flip flop based one[5], they are

1) Synthesis based method
2) Data-driven method
3) Auto-Gated Flip-Flop(AGFF)

In the synthesis method, the clock pulses that used for driving the flip-flops are excess [5]. The second, data driven method removes whatever the demerits of first method and saves higher power, which is shown in Fig.6. But its implementation is complex and is depending on the applications. The third method, Auto-gated Flip-Flop (AGFF) saves much better power comparing to the first two[5-8], which is shown in Fig.7.

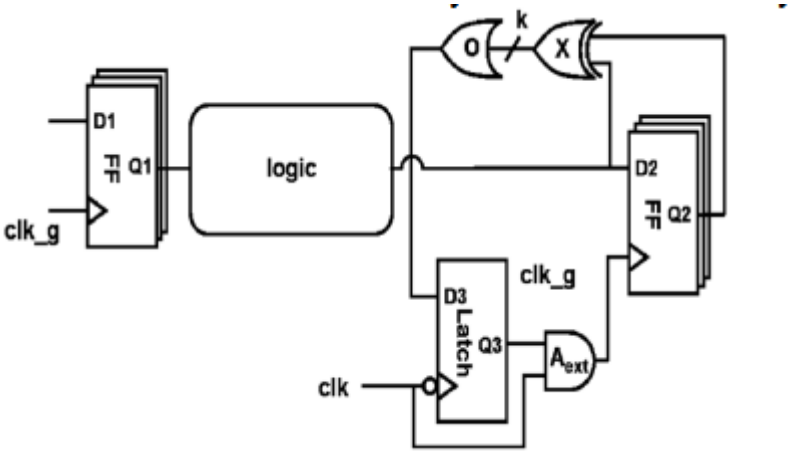

Fig. 6: Data-driven method

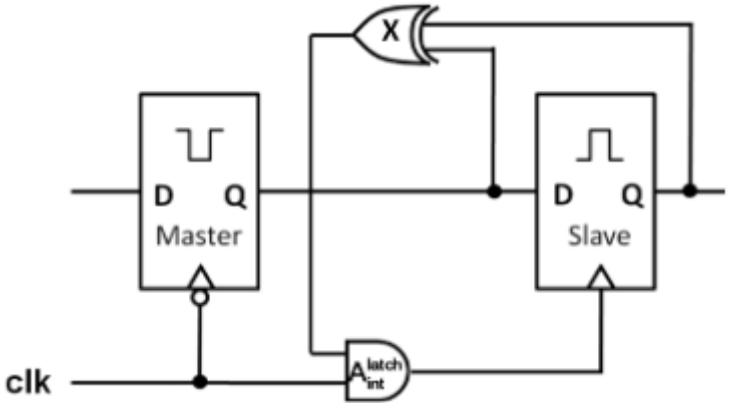

Fig. 7: An Auto–gated flip-flop

Look-Ahead Clock Gating (LACG) technique combines the all features of the above. It help to compute the enabling clock pulses of each flip-flop one cycle before the time, based on the present cycle data of those flip-flop on which it depends.

It help to stop the excess clock pulses. It has a big advantage of avoiding a tight time control of Auto-Gated Flip-Flop and data driven method, by providing a full clock cycle for enabling signals.

The basic circuit needed for Look-Ahead Clock Gating (LACG) is the Auto Gated Flip-Flop (AGFF) [9]. In the AGFF, the master latch become transparent on the falling edge of the clock. When the master latch become opaque and XOR gate indicate whether or not the slave latch should change its state. If it does not it's clock pulse is stopped and otherwise it is passed. The input of the flip-flop depends on the output of it's predecessor in the register. In AGFF , only the slave latches are gated ,leaving half of the clock load not gated. Serious timing controls are imposed on the flip flops residing on critical paths, which avoid their gating.

LACG addresses three goals, stops the clock pulses also in master latches, making it applicable for large and general designs. It help to avoid tight time controls [9]. LACG based on using XOR output as shown in Fig.7 to generate enabling clock signals of the other FF in the systems, whose data depends on that FF. The XOR output is valid only during rising clock edge. After a delay XOR output is corrupted and turns to zero. When it is latched it is valid during the entire positive half cycle which is shown in Fig. 8(a) and it's symbol is shown in Fig. 8(b). By gating the clock input, the power consumed by the new latch can be reduced. A general logic of LACG is shown in Fig.9.

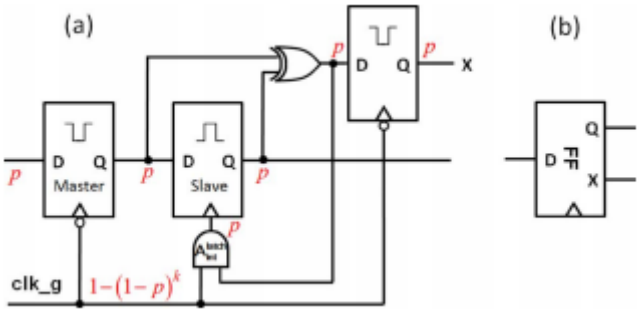

Fig.8: Enhanced Auto gated Flip-flop with XOR output used for LACG

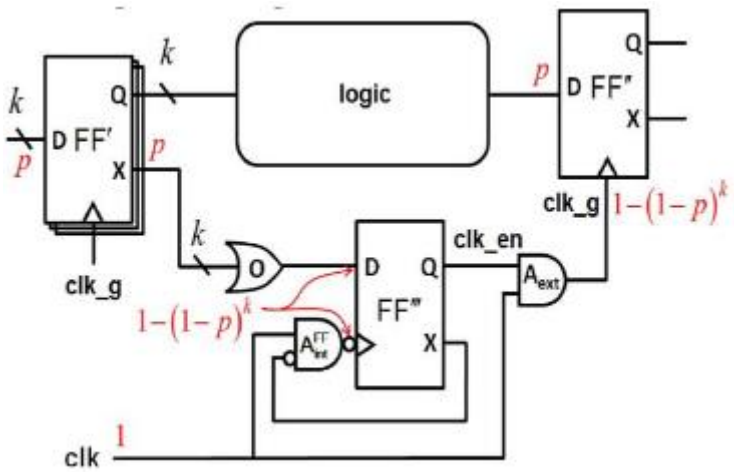

Fig. 9: A general logic for LACG.

II LOOK AHEAD CLOCK GATING FOR ULTRA LOW POWER TRANSCEIVER

Look Ahead Clock Gating can apply to the WBAN ultra low power transceiver. The Basic block diagram of transceiver is shown in Fig.10. Most of the transceivers are developed with high power consumption and high data rate. Recently the designers developed the transceivers with low data rate and low power consumption. They can provide the satisfactory performance. The data rate is 250 Kb/s. It can applied to the indoor applications of WBAN and it's working range is 1-5m. The ASIC architecture can provide low power and low complex architecture [10]. The Physical layer architecture can reduce the complexity of base band processing and maintains satisfactory performance.

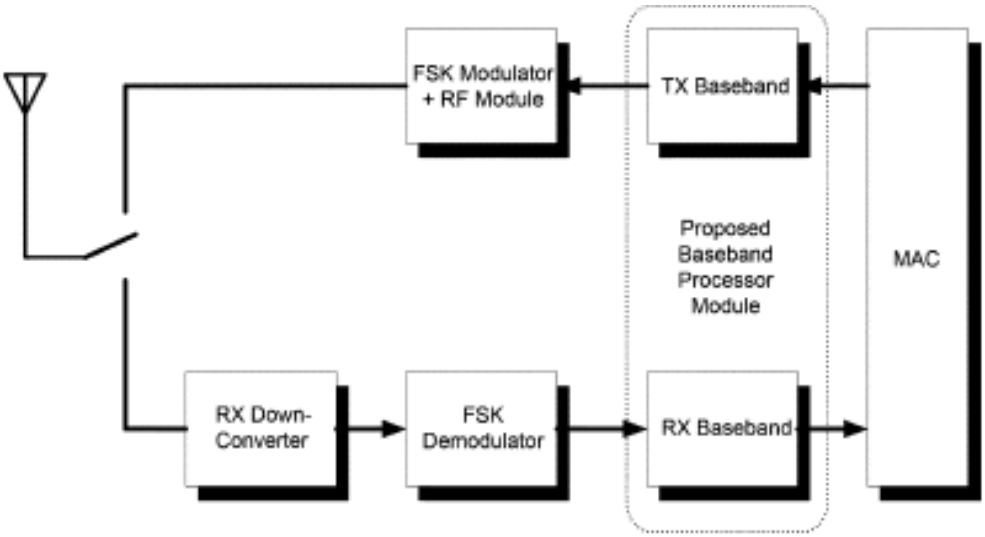

Figure 10: The basic WBAN transceiver.

Physical layer Service Data Unit (PSDU) from MAC layer is processed by the Transmitter (TX) baseband processor and produces the Physical layer Protocol Data Unit (PPDU). Signal processing and channel coding are performed on PPDU by transmitter baseband processor. 250Kb/S is the data rate of the TX baseband processor section. Transmitted data is modulated by the FSK and is up-converted into 2.45GHz RF signal. In the Receiver (RX) station, the incoming signal is down converted into 2MHz Intermediate Frequency (IF) and demodulated by the FSK demodulator. The demodulated signal is processed by the Receiver (RX) base band processor. After that, the generated PSDU is fed in to MAC layer.

III BLOCK DIAGRAM OF ULTRA LOW POWER TRANSMITTER

Low power consumption is provided by the low complexity PHY architecture. The proposed block diagram of transmitter is provided in Fig.11(a). The Transmitter (TX) receives the Physical Layer Data Service Unit (PSDU) from the MAC layer and constructs Physical Layer Protocol Data Unit (PPDU), whose structure is shown in Fig. 11(b). 127 octets is the length of the PSDU [10]. When the MAC layer produces the PSDU and fed it into (Transmitter First-in-First-out) TXFIFO and ready for the transmission.

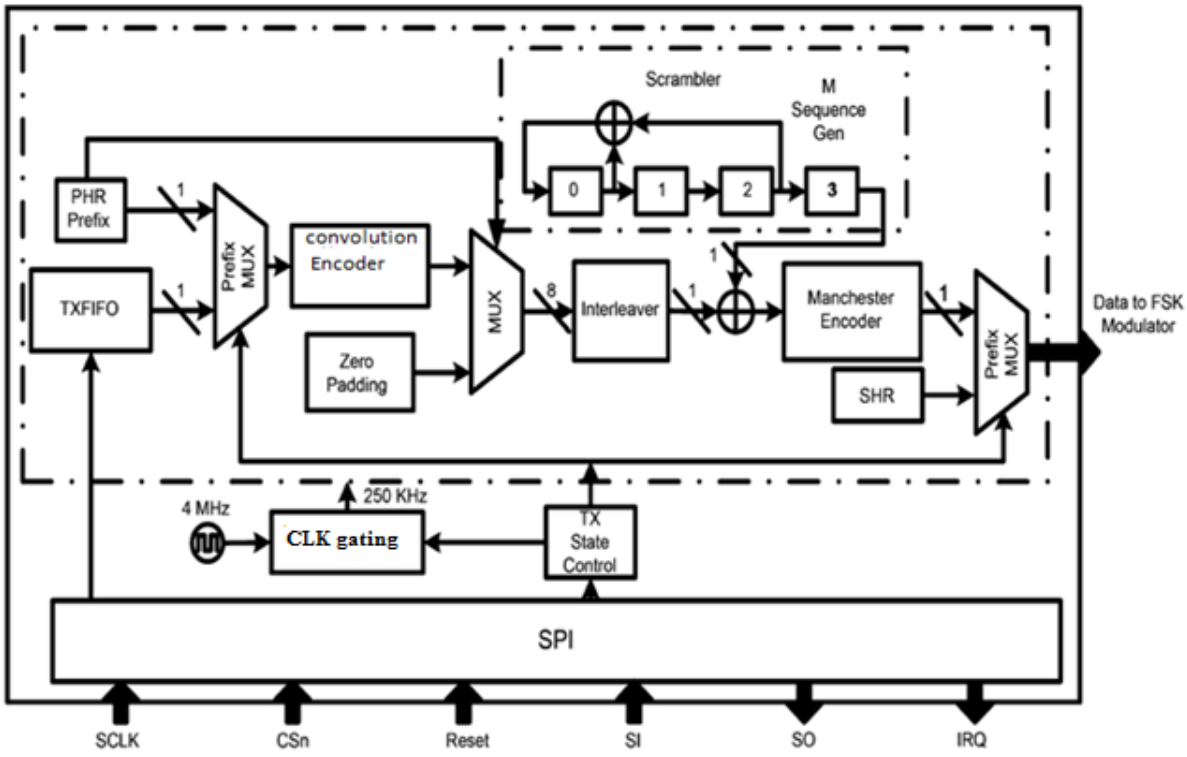

Fig 11(a): WBAN transmitter with Look Ahead Clock Gating

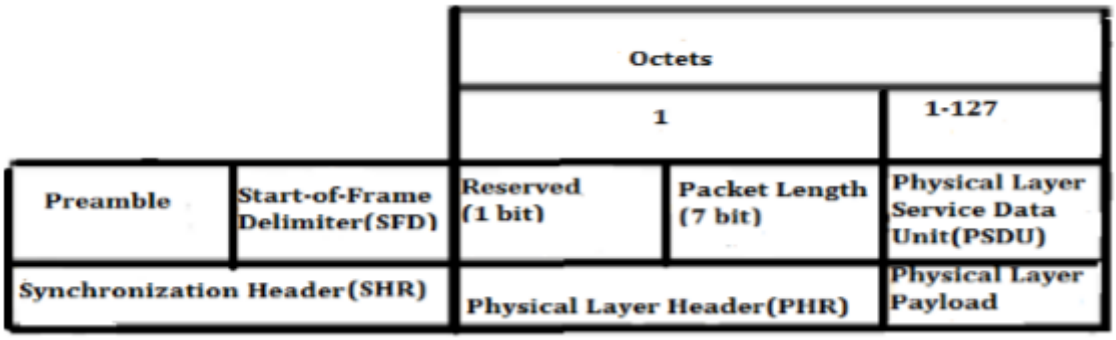

Fig 11(b): PPDU packet format

The Transmitter(TX) state control block controls the Prefix MUX ,which help to select the input to the convolution encoder. when the transmission command is enabled by the MAC layer, PHY header(PHR) is preixed to the PSDU and passed into the convolution encoder. Convolution encoder is a forward error correction code, that can generate parity symbols.In the transmitter module the input to the convolution encoder is 4 bit and convert it into an 8 bit code[11]. The input of the convolution encoder is of one bit word length. For each consecutive input data of 4 bit, convolution encoder generates 8 bit code.

The output from the convolution encoder send to interleaver. It helps to eliminate long strings of like bits and helps to remove most periodic patterns that can produce undesirable frequency components. The interleaved data sends to the scrambler. The output of scrambler is a serial bit of code. The output of srambler XORed with the output of interleaver.

The XORed data send to Manchester encoder. The Manchester encoder codes bit “0” into “01” and bit “1” into “10”. So total number of “0” and “1” are balanced. The output of Manchester encoder is prefixed with Synchronization Header (SHR) and sends to FSK modulator.

IV BLOCK DIAGRAM OF ULTRA LOW POWER RECEIVER

Block diagram of receiver is shown in Fig.12. The FSK demodulator demodulate the received data stream[8-9]. D flip-flop is used to sample and restore the analog signal. When the voltage of the input ignal is greater than the Voltage High-Low(V_{HL}) of the D flip-flop, then the output is”1”. When the voltage of the input ignal is lower than the Voltage Low- High (V_{LH}) of the D flip-flop, then the output is”0”. As shown in Figure.12, the signal is first fed into the Synchronization and Data Recovery (SDR) block to recover the received data. Using a shift register matrix block SDR over-samples the incoming signals. It helps to calculate the correlation between the incoming data and predefine preamble sequence to get the synchronization.

The signals are first serially fed into the synchronization and data recovery (SDR) block to achieve synchronization and to recover the received data. The SDR block over-samples the incoming signal using a shift register matrix block and calculates the correlation between the incoming data and the predefined preamble sequence to achieve bit synchronization. This helps to detect continuously the peak of the calculated correlation. When the peak value is detected, Start-of-Frame Delimiter (SFD) correlator helps to calculate the correlation between incoming data and predefined SFD sequence. The peak value is continuously monitored by peak detector.

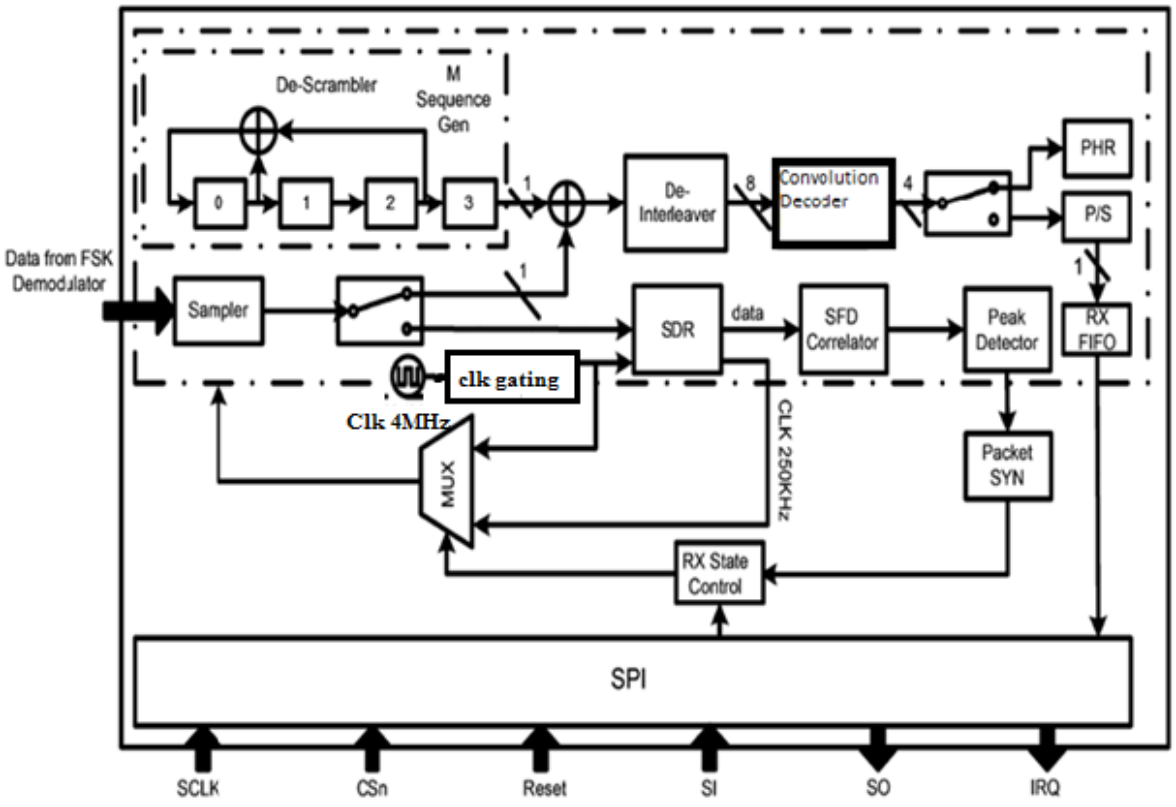

Fig.12 : Block diagram of Ultra Low Power Receiver

Once the peak value is detected, packet synchronization is confirmed. The preamble sequence and Start-of- Frame Delimiter (SFD) are removed. The Packet SYN block indicates to the receiver state control block that the correct PHR and PSDU are received. The 250kHz clock is generated by the SDR block. The Receiver (RX) state control box select the operating frequency of the receiver base band processor, that can be between 250KHz and 4MHz frequency.

Manchester decoding is performed on the received PSDU and PHR stream by detecting first bit or every two received continuous bits. After that incoming data is desrambled,which is the opposite action of scrambler[10]. The output of the descrambler is 1 bit word length and XOR operation is performed with the incoming data bit by bit. After that FEC decoding is performed on the PHR and PSDU data stream. The Forward Error Correction (FEC) block include the deinterleavind and convolution decoder block. The output of the deinterleaver is of 8 bit word length and after that the output is fed to convolution decoder. Convolution decoder check whether there is any error in the incoming data and correct the error. If the convolution decoder cannot correct the error, the receiver stop the receiving of further data. The MAC layer request the retransmission of the packet. The PHR is decoded first.The length of the PSDU is obtained by the receiver(RX) state control block. The word length of the convolution decoder output is 4 bit. There is a parallel to serial buffer, the bits in the PSDU is fed in to the Receiver First-In-First-Out(RXFIFO) in serial sequence with 1 bit word length and it is read by the MAC layer.

V SIMULATION OUTPUT

A. Transmitter output using Hamming encoder without clock gating

Fig.13(a) and (b) shows that the output wave form and the output power of ultra low power transmitter(TX) using hamming encoder without clock gating.

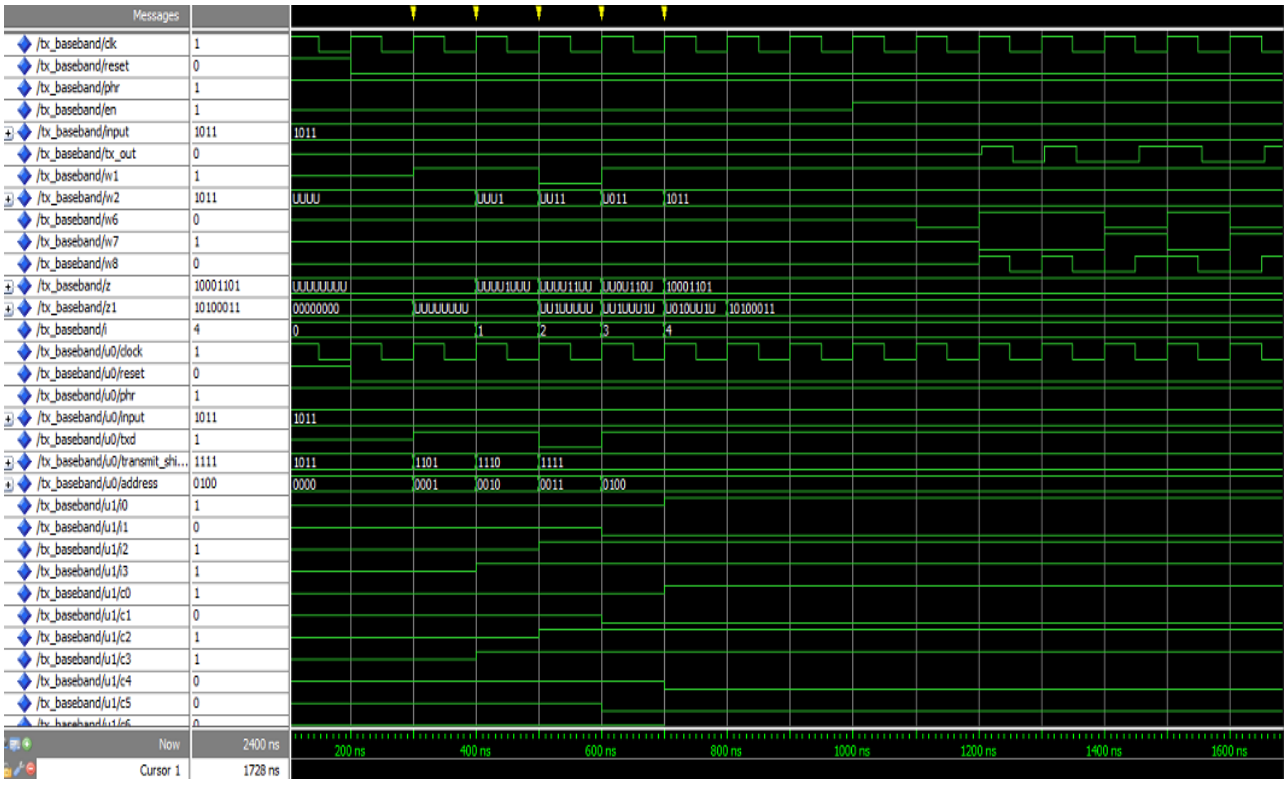

Fig.13(a): Output wave forms of Ultra Low Power TX using Hamming encoder without clock gating

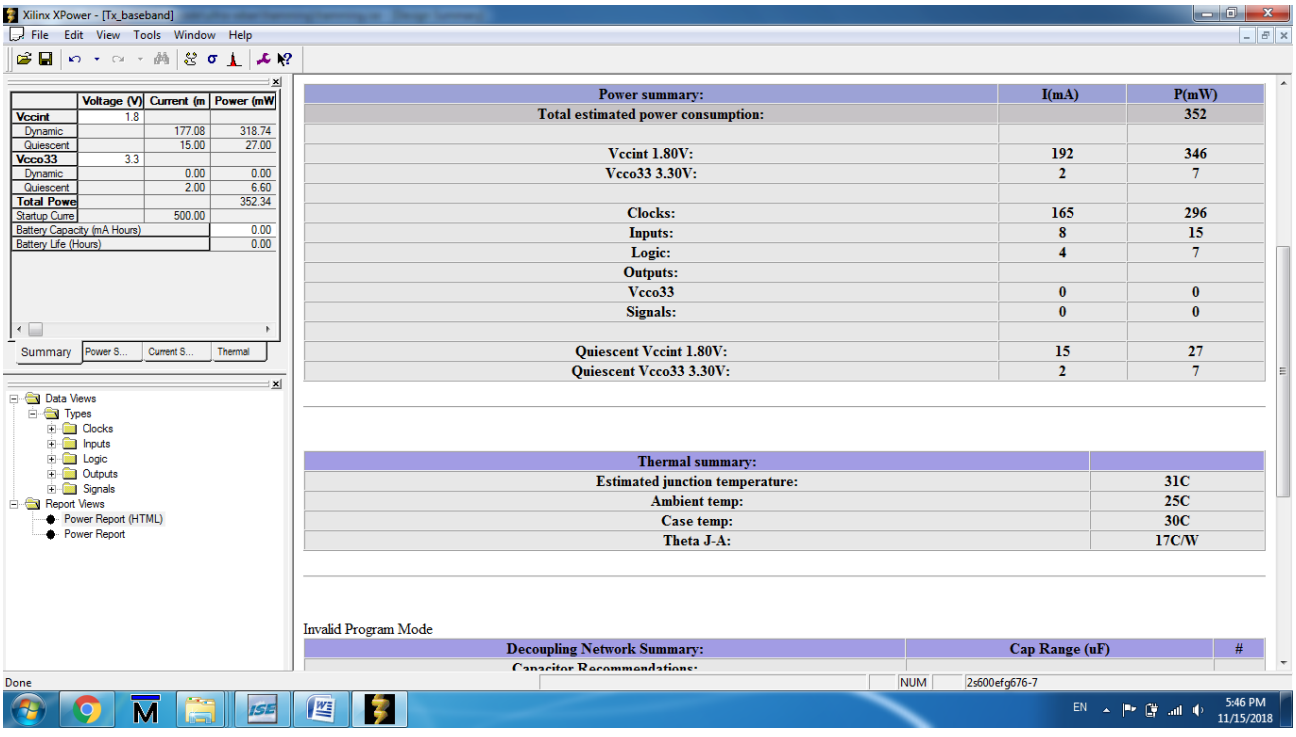

Fig. 13(b): Output power of Ultra Low Power TX using Hamming encoder without clock gating

B. Receiver output using Hamming decoder without clock gating

Fig.14(a) and (b), shows the output wave form and output power of ultra low power receiver using Hamming decoder without clock gating.

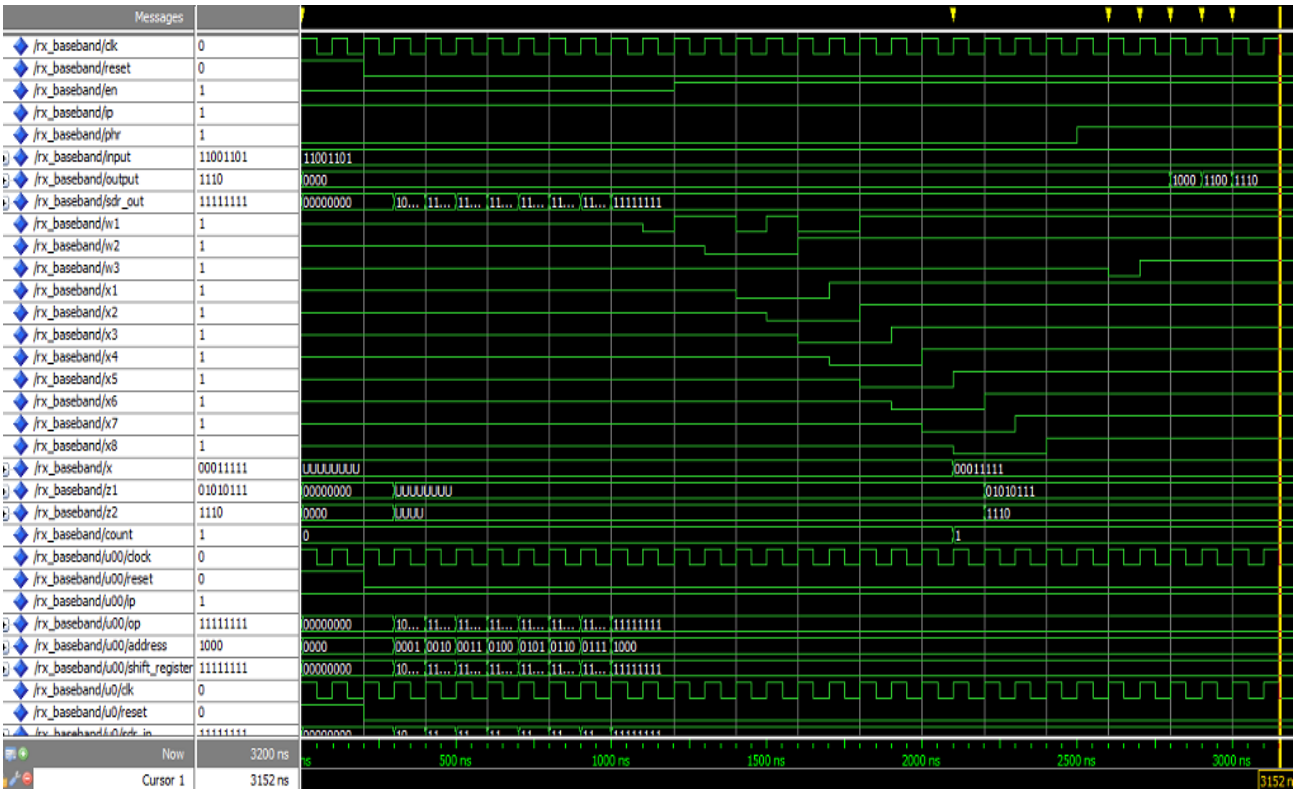

Fig.14(a): Output wave form of receiver using Hamming decoder without clock gating

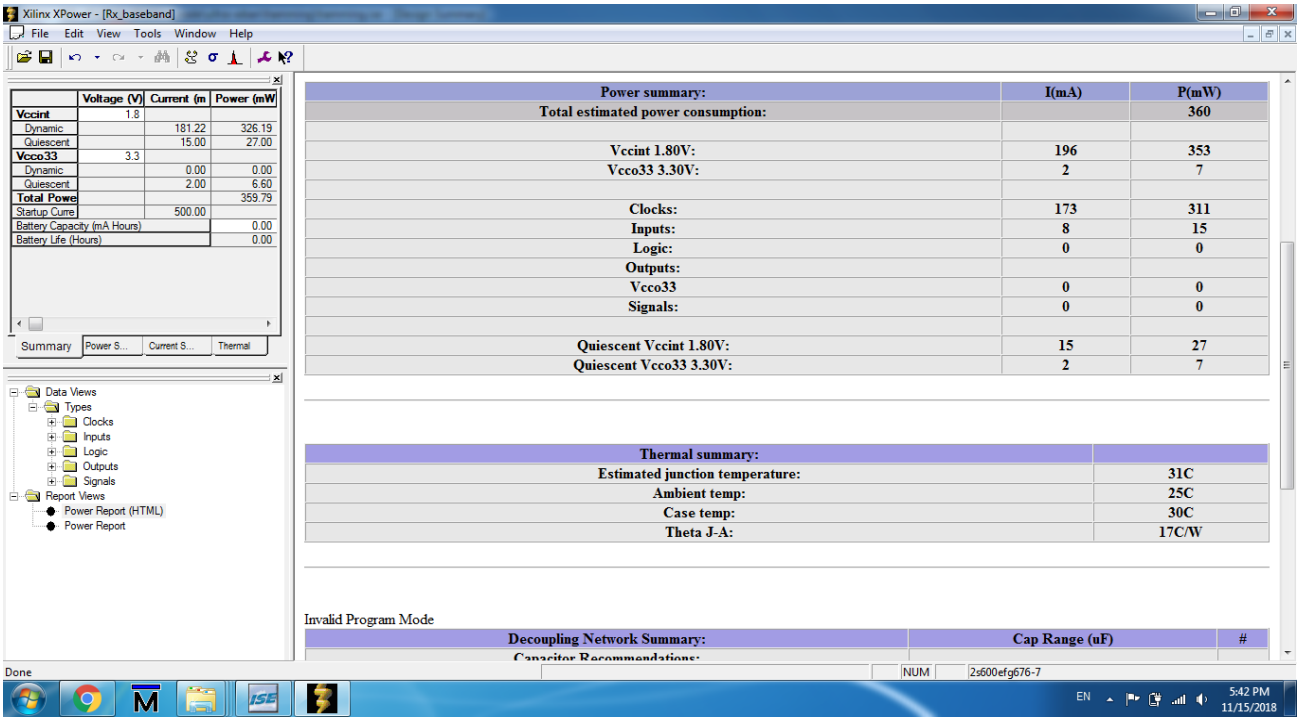

Fig. 14(b) : Output power of Ultra Low Power RX using Hamming decoder without clock gating

C. Transmitter output using convolution encoder without clock gating

Fig.15(a) and (b) shows the output wave form and output power of ultra low power transmitter using convolution encoder without clock gating.

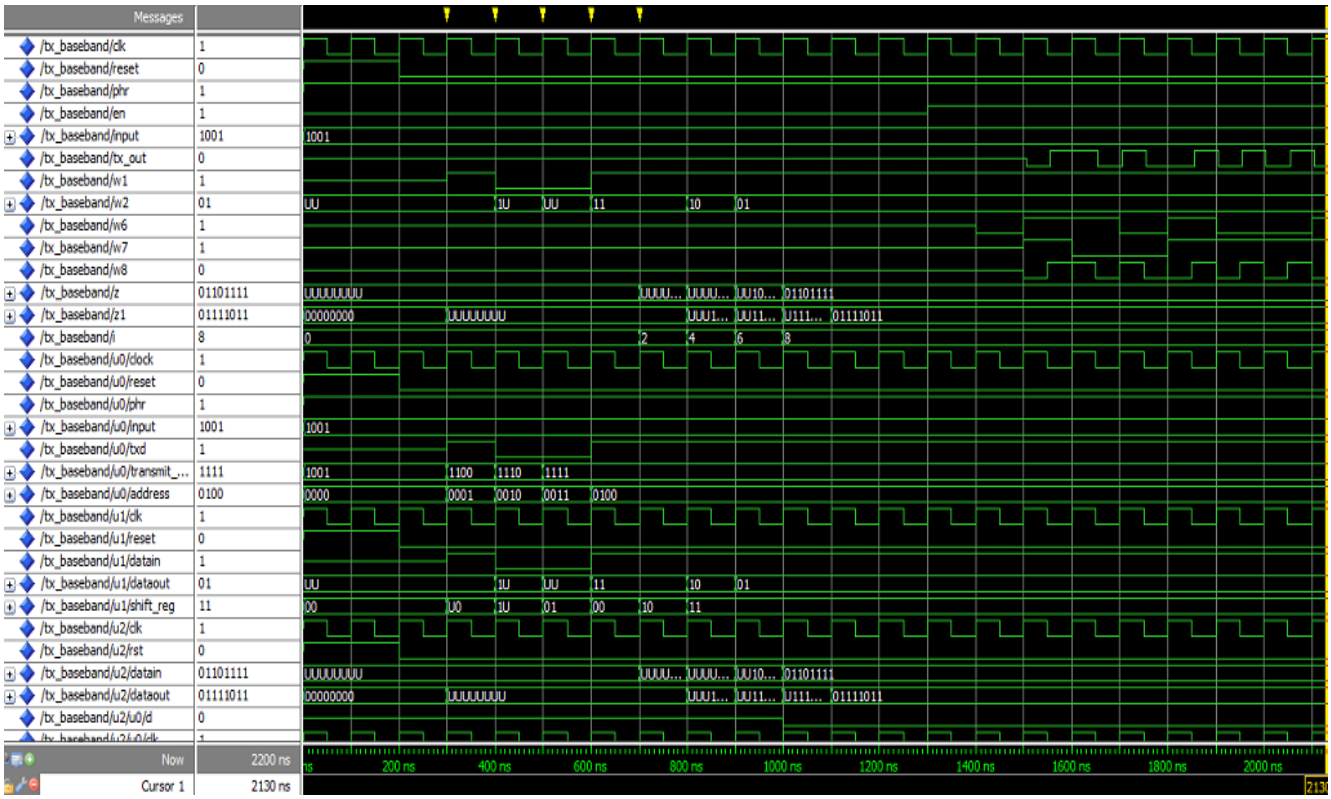

Figure 15(a): Output wave forms of Ultra Low Power TX using convolution encoder without clock gating

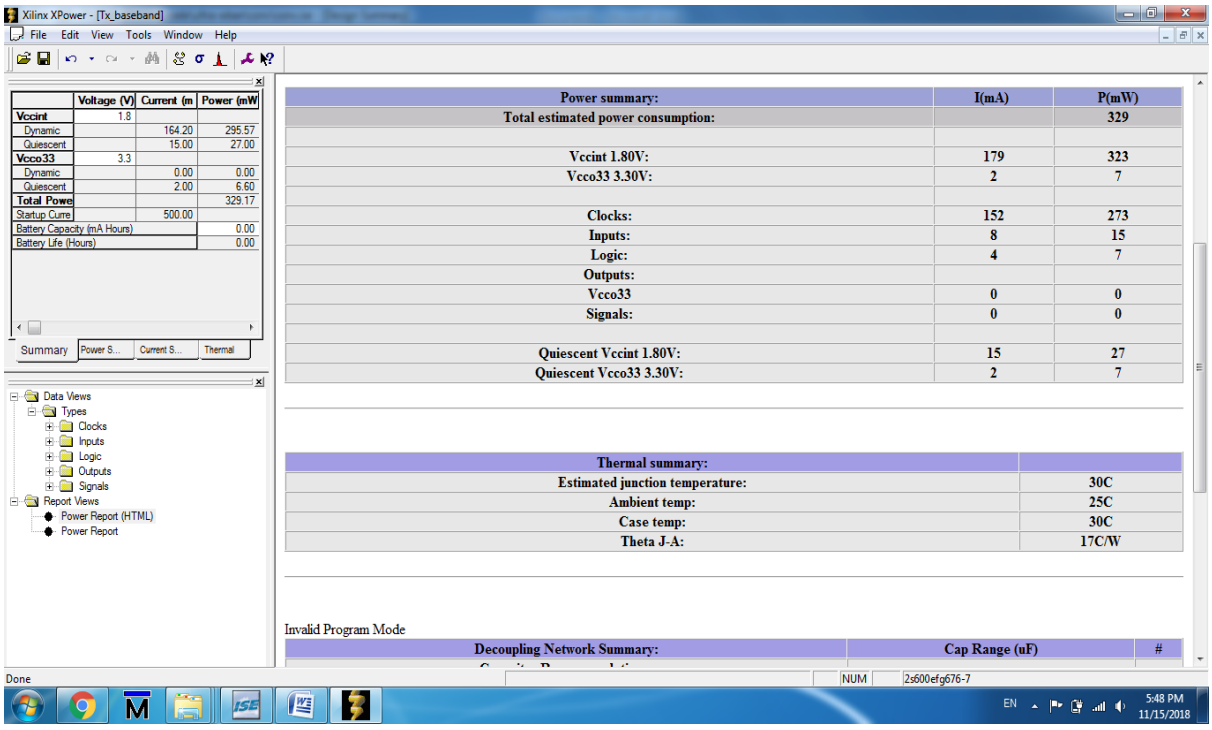

Fig. 15(b): Output power of Ultra Low Power TX using convolution encoder without clock gating

D. Receiver output using convolution decoder without clock gating

Fig.16(a) and (b) shows the output wave form and output power of ultra low power receiver using convolution decoder without clock gating.

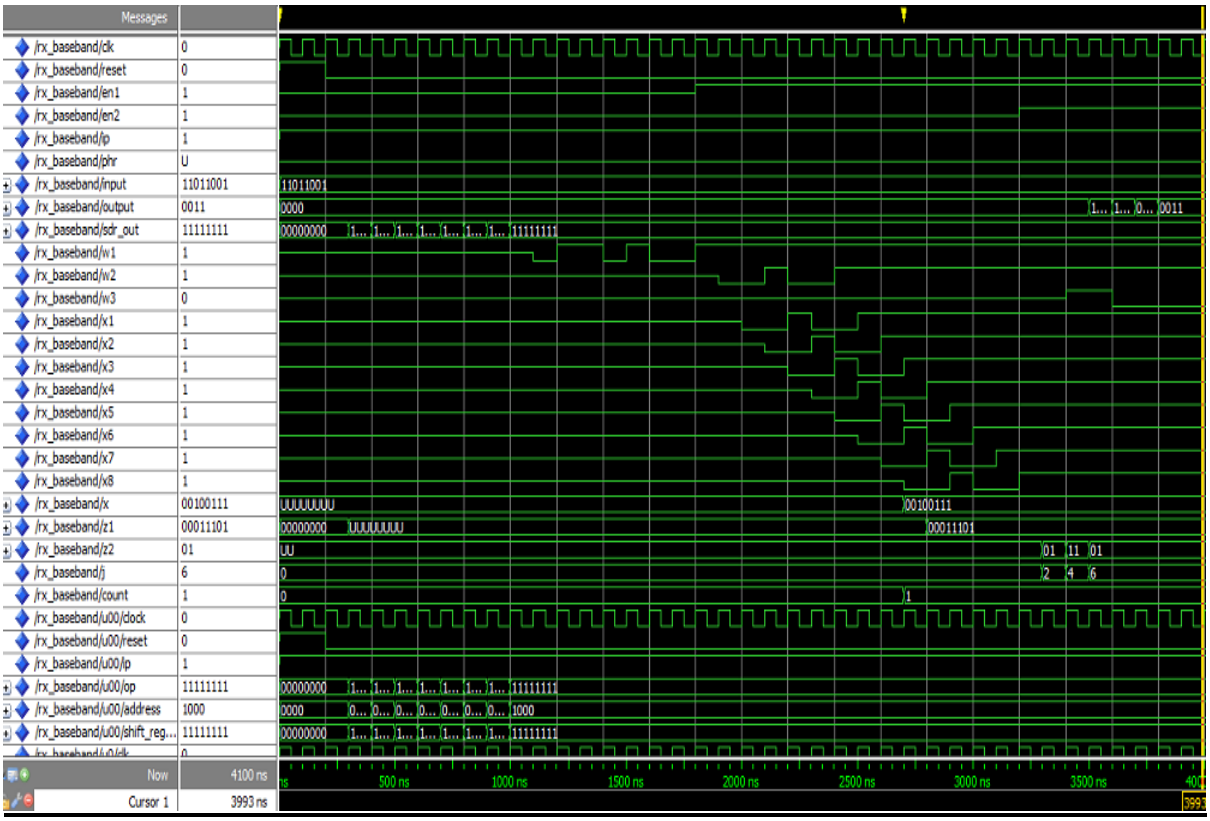

Fig. 16(a): Output wave form of receiver using Convolution decoder without clock gating

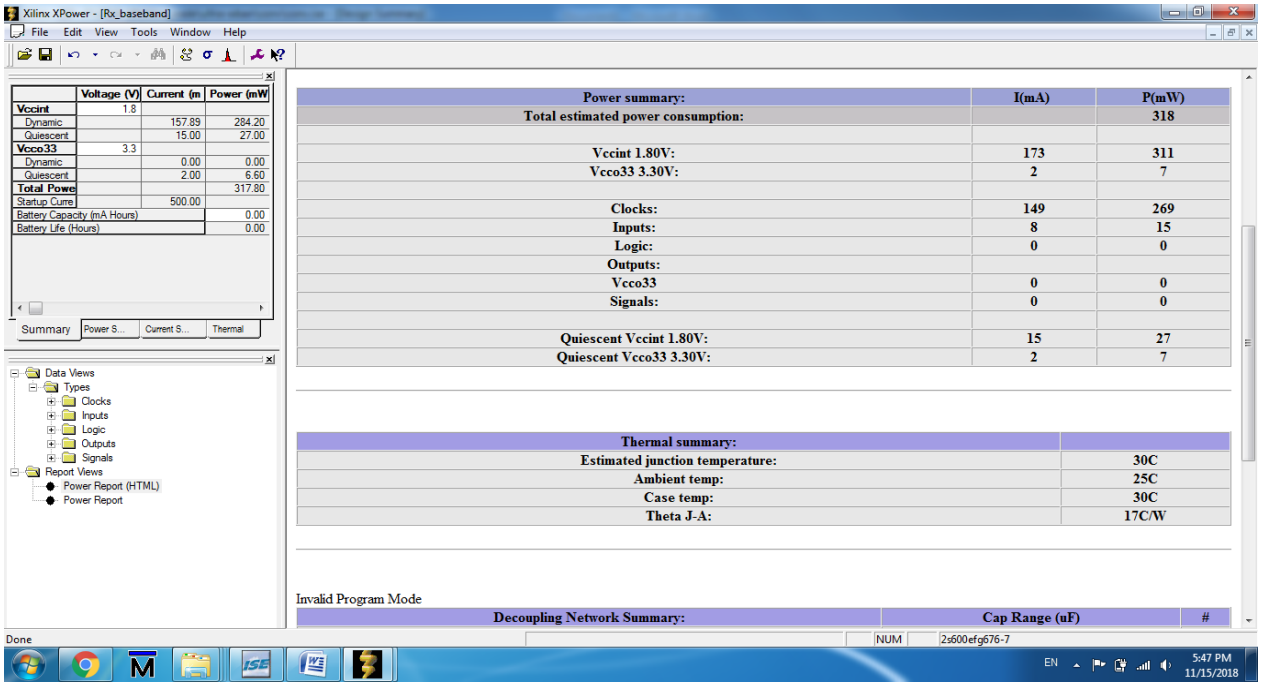

Fig.16(b) : Output power of Ultra Low Power RX using convolution decoder without clock gating

E . Transmitter output using Convolution encoder with clock gating

Fig.17(a) and (b) shows the output wave form and power of Ultra Low Power transmitter using convolution encoder with clock gating.

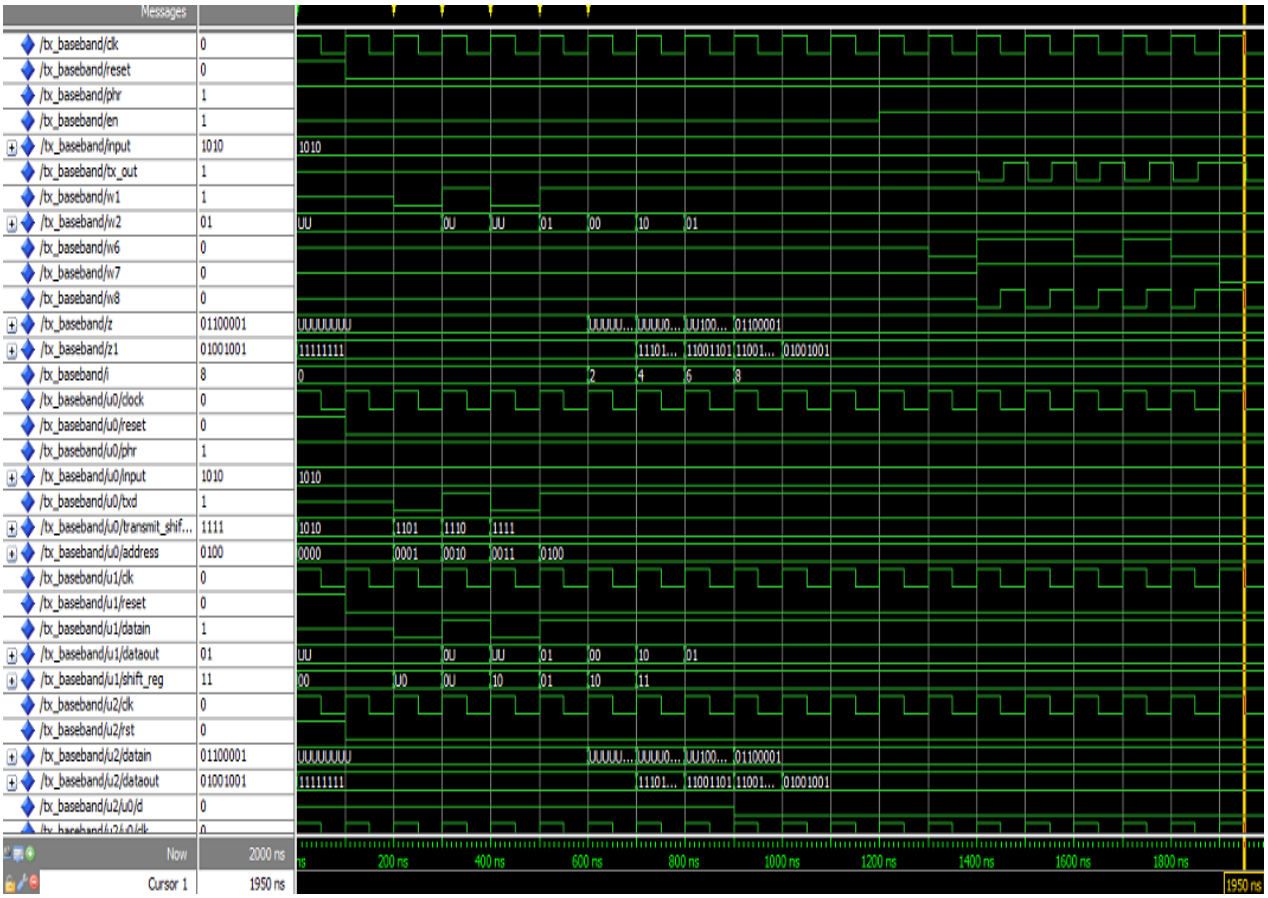

Fig.17(a) : Output wave forms of Ultra Low Power TX using Convolution encoder with clock gating

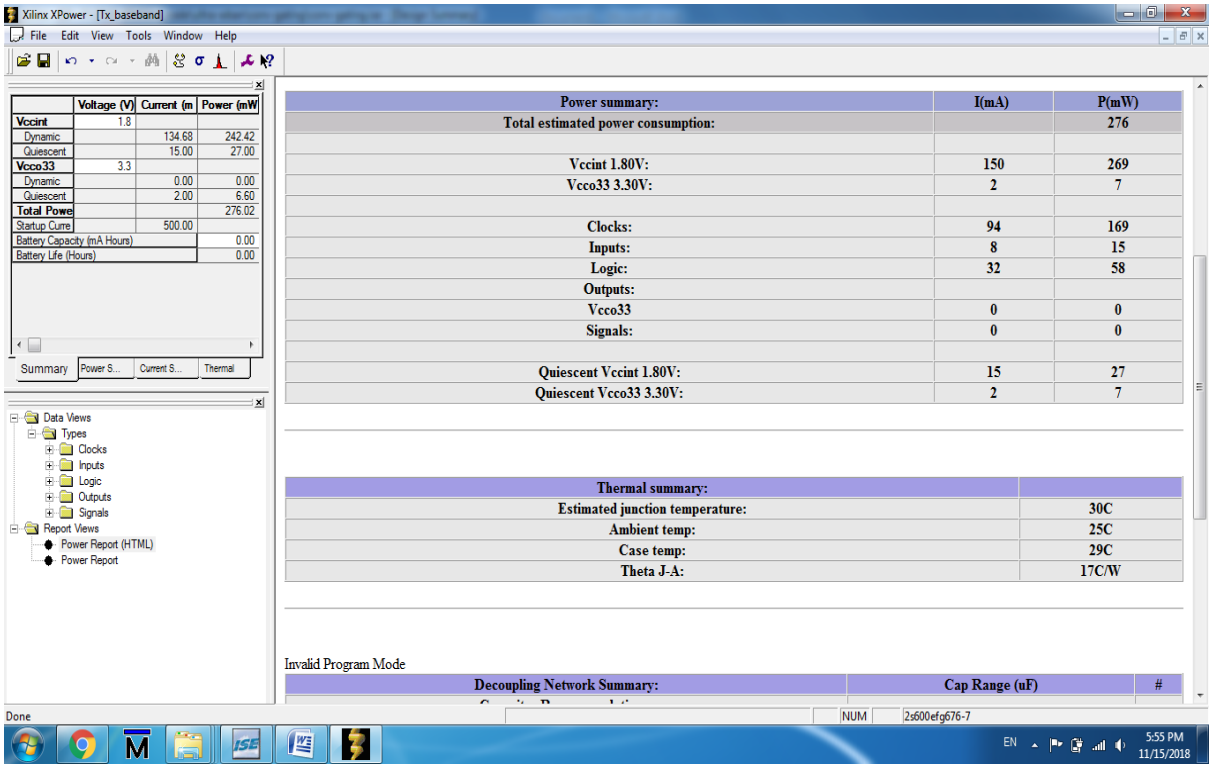

Fig.17(b) : Output power of Ultra Low Power TX using convolution encoder with clock gating

F. Receiver output using convolution decoder with clock gating

Fig:18(a) and (b) shows the output wave form and output power of Ultra Low Power receiver using convolution decoder with clock gating.

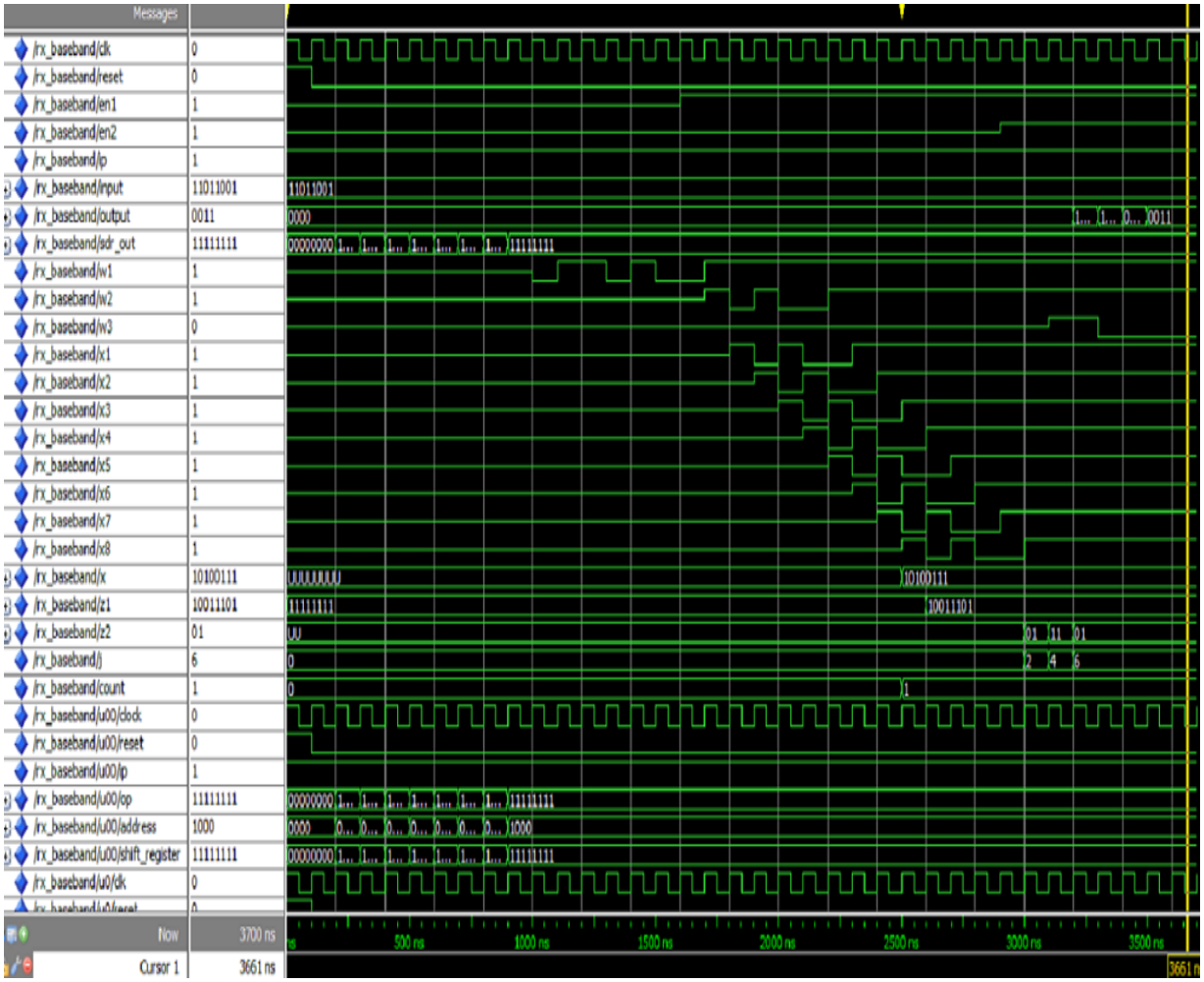

Fig.18(a) : Output waveform of Ultra Low Power RX using convolution decoder with clock gating

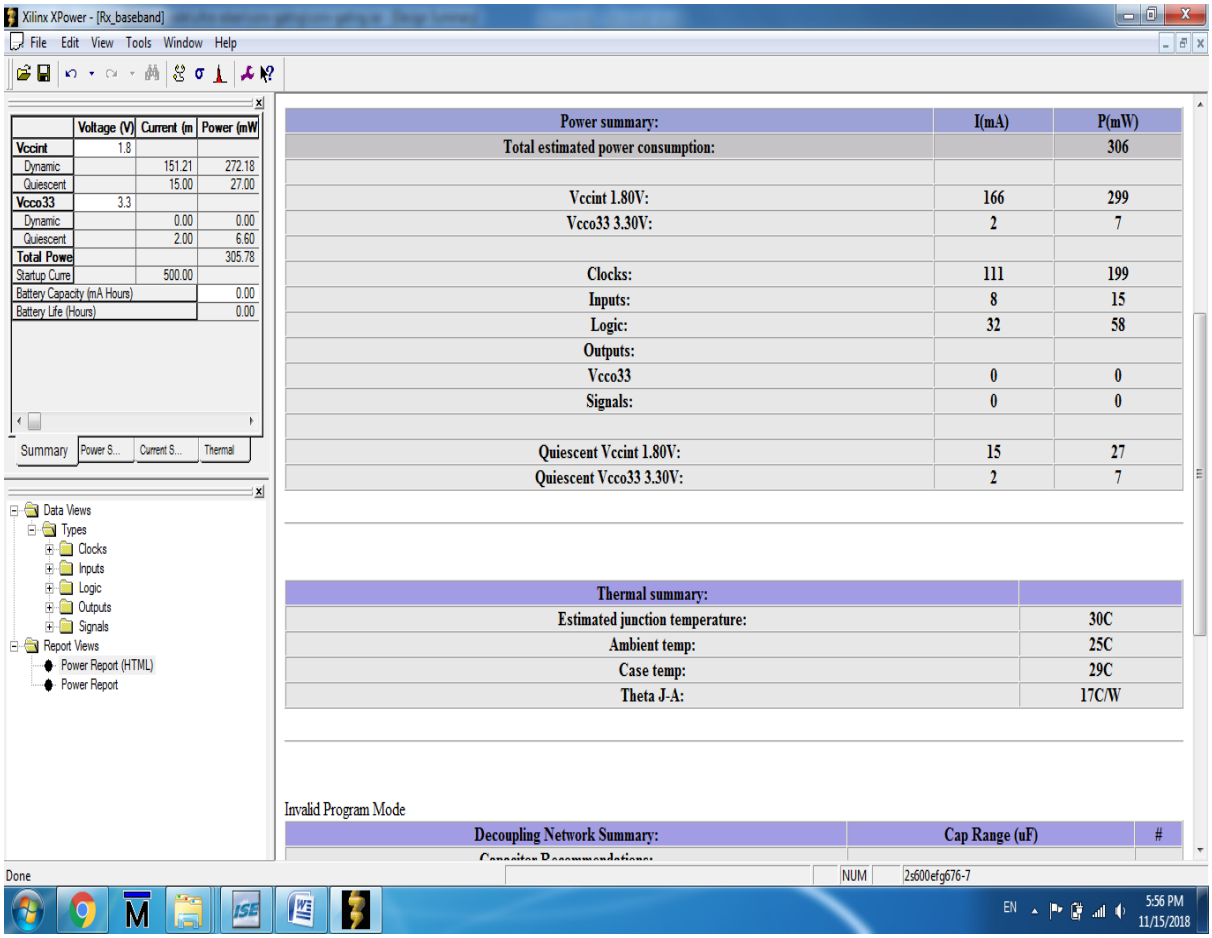

Fig.18(b) : Output power of Ultra Low Power RX using convolution decoder with clock gating

VI. CONCLUSION

Look Ahead Clock Gating is used for the better performance of Ultra Low Power Transceiver.This method helps to decrease the power of the entire circuit by controlling the clock input to the circuit. ASIC architectur is used here. The clock input to the circuit is 4MHZ. The output power comparison is done with and with out clock gating. The convolution encoder with clock gating helps to decrease the power of the entire circuit very well.

References

[1] Priya Singh, Ravi Goel, *Clock Gating: A Comprehensive Power Optimization Technique for Sequential Circuits*. "International Journal of Advanced Researchin Computer Science & Technology, Vol. 2, Issue 2, April - June 2014, pp 321-324

[2] Harpreet Singh, Dr. Sukhwinder Singh. *A Review on Clock Gating Methodologies for power minimization in VLSI circuits.* International Journal of Scientific Engineering and Applied Science Volume-2, Issue-1, January 2016, pp 298-305.

[3] Jagrit kathuria , M.Ayoubkhan ,Arti Noor, *A Review of Clock Gating Techniques* International Journal of Electronics and Communication Engineering Vol.1.No.2.Aug 2011, pp106-114.

[4] . Mayuri B. Junghare, Aparna S. Shinde. *A Clock Gating Technique Using Auto Gated Flip Flop for Look Ahead Clock Gating.* International Journal of Science and Research. Volume 4, Issue 7, July 2015 pp1525-1530.

[5] Nandita Srinivasan, Navamitha.S.Prakash, Shalakha.D, Sivaranjani.D, Swetha Sri Lakshmi.G, B.Bala Tripura Sundari, *Power Reduction by Clock Gating Technique*, ScienceDirect, Procedia Technology 21, 2015, pp 631 – 635.

[6] Priyanka Saraswat, Mrs. Tanu Goyal, *Novel Methods Of Clock Gating Techniques: A Review* , International Research Journal of Engineering and Technology Volume.05 Issue: 01,Jan-2018, pp 21-25.

[7] Ms. Aparna B, Mr. Arul Kumar M. *Low Power Auto Gated Flip-Flop Design using Clock Gating Technique* , Dept. of Electronics and communication , Nehru Institute of Technology . Volume 4, Issue 3, March 2015, pp-192-196.

[8] S.V.Lakshmi , P.S.Vishnu Priya, Mrs.S.Prema *Performance Comparison of Various Clock Gating Techniques* ,. IOSR Journal of VLSI and Signal Processing Volume 5, Issue 1,Jan - Feb. 2015, pp 15-20 .

[9] Shmuel Wimer, and Arye Albahari. *A Look-Ahead Clock Gating Based on Auto-Gated Flip-Flops* IEEE transactions on circuits and systems—:regular papers, Vol.61, no.5, May 2014, pp 1465-1472.

[10] Xin Liu, Yuanjin Zheng, Bin Zhao, Yisheng Wang, and Myint Wai Phyu. *An Ultra Low Power Baseband Transceiver IC for Wireless Body Area Network n 0.18-m CMOS Technology***,** IEEE transactions on Very Large Scale Integration (VLSI) systems, Vol. 19, no. 8, august 2011, pp 1418-1428.

[11] S. Sindhu, A. Balamurugan *Convolution Code For Better Performance Of Ultra Low Power Transceiver*, International Journal of Engineering and Techniques - Volume 4 Issue 2, April-2018, pp 938-948.